Department of Precision and Microsystems Engineering

Exploring Silicon Photonics to Sense Two-Dimensional Membrane Mechanics

Asgeir

Report no : 2023.055
Coach : R.T. Erdoğan
Professor : Dr. G.J. Verbiest & Dr.ir. W.J. Westerveld
Specialisation : Optomechatronics/Mechatronic System Design
Type of report : MSc. Thesis
Date : 21-08-2023

Delft University of Technology

Exploring Silicon Photonics to Sense Two-Dimensional Membrane Mechanics

by

Ásgeir Ísak Þrastarson

To be Defended on August 21, 2023 at 9:30 am.

Student number: 5141400

Supervisors:
Gerard Verbiest
Wouter Westerveld

Abstract

Silicon photonics have received more attention in recent years due to further development in CMOS manufacturing methods. The development allows silicon photonics to be smaller than ever before. This leads to smaller silicon photonic devices that can transceive light, which is typically done at a wavelength of $1550nm$ for silicon photonics. A silicon photonic device that benefits from this wavelength is the silicon waveguide, which can transceive light by being coupled to other waveguides. When the second guide is later coupled back with the main waveguide, a resonance can form between the guides. This can turn the silicon waveguide in to a sensor that relies on interference from the recoupled signal. The design used for this study has the waveguides in a relatively deep trench, which means that a membrane can be suspended above the waveguides. In theory the membrane should reflect some of the light that escapes from the waveguide back. In this work membranes made from graphene and molybdenum disulfide are suspended over a silicon waveguide in hopes to detect the motion of the membrane. A proof of concept by experimenting with membranes integrated on silicon photonics can give way for a new type of sensor, which is both microscopic and has a high signal-to-noise ratio. The experiments are conducted by propagating light through the waveguide, the light should then interact with the suspended membrane on top. The first indication that the concept was possible was when a transmission graph that swept the light's wavelength around $1550nm$ changed after introducing a suspended membrane over the waveguide. The change showed that waveguides react to membranes over them without eliminating the transmission altogether. This is a great step when it comes to a proof for the concept. However, it is still needed to take a frequency measurement before the concept has been fully proofed.

Contents

1 Introduction

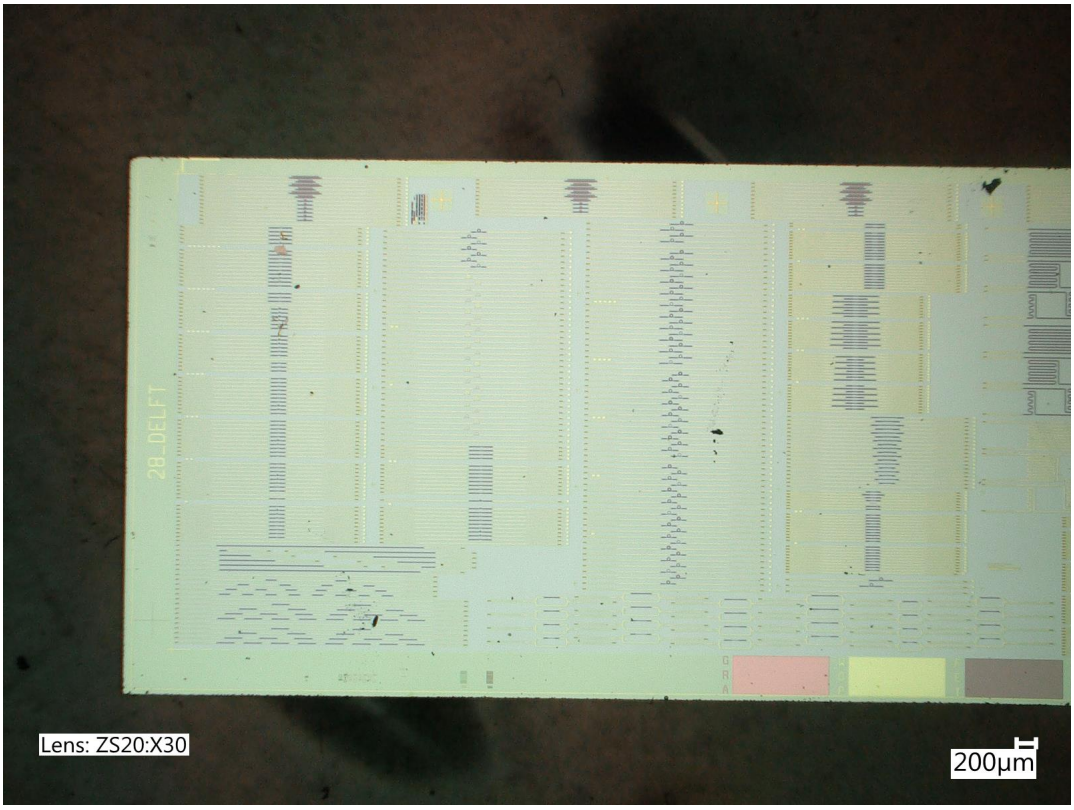

Figure 1: The silicon photonic chip used throughout this study. The left to center-right side of the silicon chip can be seen here. The circular and doughnut devices are in the first three central columns from the left. The left most column exclusively contains circular devices The center column starts with doughnut shaped devices and ends with circular devices and the final column is exclusively for doughnut shaped devices. Other devices seen in the figure are, bus ring resonators on top with corresponding coupling gaps with a single ring resonator below the bus. A series of short straight waveguides are under the first column, these guides are used to measure internal transmission losses. Right of the short waveguides, are Mach-Zehnder interferometers. The fourth column contains a mixture of Bragg gratings and bus ring resonators with two doughnut membranes at the bottom.

Two-dimensional (2D) materials have become a more relevant research topic in recent years and it started with A. K. Geim & K. S. Novoselov when they rediscovered graphene [7]. 2D materials are atomically thin, they can therefore make smaller sensors with higher natural frequency due to their small size, low mass, and high elasticity. In other words, the low stiffness and mass makes 2D materials resonate in the megahertz (MHz) range [8]. The high natural frequency means that it is possible to detect high frequencies with a large signal to noise ratio (SNR).

Silicon photonics is the study of light by using silicon as a medium to transceive light. The transceiver can be used as a waveguide to propagate light. Furthermore, the waveguide can be integrated to an interferometer which turns the guide into a sensor, e.g., a waveguide coupled to a ring resonator can be used as a microphone by having the light propagating through the ring. Such a sensor using a ring resonator has been used to detect the motion for a carbon nanotube [1]. A sensor that combines silicon photonics and 2D materials can be used to detect small changes in sound and could be used to develop a new type of microphone or an ultrasound sensor. Furthermore, this detection method can mass produce sensors with a radius as small as

$10\mu m$ while still having a large SNR which will be discussed later in the report.

The sensors are made by suspending 2D membranes over silicon waveguides. However, the waveguide does not provide the sensing on its own, most of the sensing comes from resonator dips, due to interfering light from integrated interferometers in the waveguide, such as ring resonators, Bragg gratings, and Mach-Zender interferometer. Where, the ring resonator has been researched for ultrasound sensing ($> 20.0kHz$) [11], [26] and, other applications such as modulation or filtering. Whereas, modern ultrasound sensors work by vibrating a magnet that converts the energy from an ultrasonic pulse to electrical energy. These ultrasonic pulses can in theory actuate a 2D membrane that is suspended over a capacitor instead of a magnet. When taking this a step further the membrane can be placed over a ring resonator, where the membrane will change the light intensity instead of the capacitance. The sensors should then detect the membrane motion instead of the pure ultrasonic pulse.

1.1 State-of-the-Art

1.1.1 Two-Dimensional Materials

A Two-dimensional material is any material that is one unit layer thick, whereas a unit is the smallest possible crystal height. They were rediscovered by A. K. Geim & K. S. Novoselov when they manged to get an atom layer of graphite on tape [7]. because 2D materials are very thin and light; a small force acting upon the material will result in a large change in its position. Moreover, their natural frequency is inversely proportional to the mass squared in the simple natural frequency formula, $f_0 = \frac{1}{2\pi}\sqrt{\frac{k}{m}}$, where k is the stiffness of the resonator and f_0 is the natural frequency. The low mass combined with a high stiffness gives an natural frequency in the mega Herz range [8]. The 2D materials used in this study are grphene and molybdenum disulfide (MoS_2), since both are readily available at TU Delft.

Graphene is the most studied 2D material, because it was the first 2D material that was fabricated. Graphene is a flat monolayer of carbon atoms tightly packed in a two-dimensional honeycomb lattice [7], [17]. The lattice can be rolled into a carbon nanotube or shaped into a ball. Furthermore, graphene is a very stiff material with a Young's modulus ranging from $E = 1.0 \pm 0.1TPa$ to $2.0 \pm 0.5TPa$ when the effective thickness is $0.335nm$ [17], [10]. However, this review will focus on the flat lattice and other characteristics of graphene. One of the reasons why graphene is used and not some other 2D material such as Molybdenum disulfide (MoS_2) is that graphene has a very stable crystalline structure [16]. However, graphene is not as perfect as it seems at first, since it has zero band gap which means that graphene is a conductive material that absorbs almost all light. Thankfully, it is possible to tune the band gap of graphene up to $1eV$ through electrical gating [16], [20].

Molybdenum disulfide is a naturally occurring material that is mainly mined as a site product from copper mining. However, the concentration of MoS_2 tents to be low which makes it easier to synthesise. There are various methods to obtain MoS_2, e.g., a chemical reaction of lithium sulfide and molybdenum chloride produces MoS_2 with a large surface area. Other methods may involve microwave plasma, prolonged heating, or pulsed laser evaporation[2]. The crystal structure is an S-M-S bond where molybdenum is sandwiched between sulfur layers, where six sulfuric atoms coordinate a single molybdenum atom. MoS_2 an anisotropic semiconductor that has a much higher electrical resistance when measuring out of plane [2]. Moreover, MoS_2 can have a band gap of $1.8ev$ [24], [3].

1.1.2 Readout Methods

There are a couple of readout methods that have been tested when it comes to measuring motion *w(x,y,t)* in 2D membranes. These methods are *optical readout*, *transconductive readout*, *capacitive readout*, and *position dependent readout* [23].

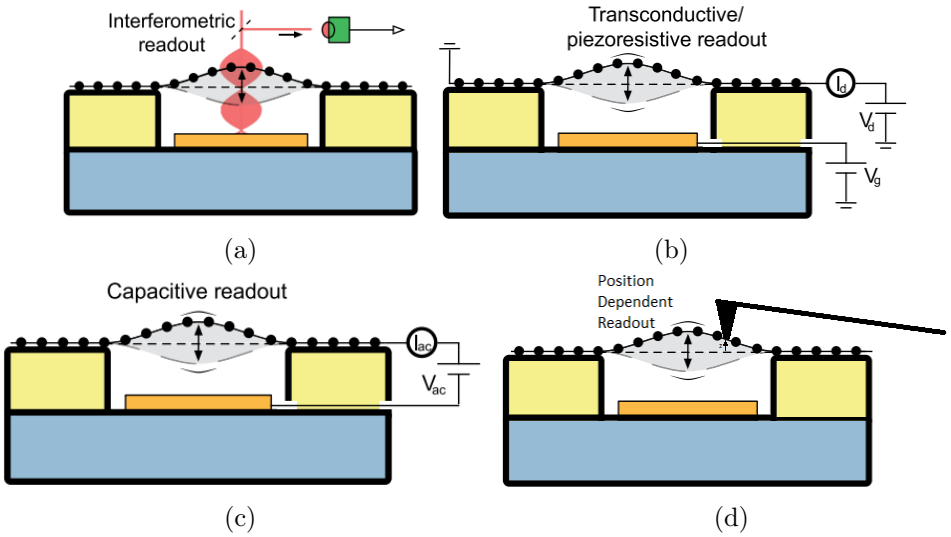

Figure 2: Existing readout methods[23].

The optical readout method relies on a laser that is reflected from he Fabry-Perot cavity formed by the semi-transparent 2D material and the underlying reflective substrate which is shown in Figure 2a. The laser measures a standing wave electric field intensity *I(z)* from the superposition of the incoming and reflected optical wave. The maximum sensitivity is achieved when the the maximum slope in the optical field intensity is $\frac{dI(z)}{dz}$. This can be calculated if the optical material properties and geometries are known [23].

There are also other optical readout methods that have been developed e.g. a Michelson interferometer setup. The advantage of this setup is that it does not need a reflective surface while the membrane is free-hanging. On the other hand, the vibrations from the interferometer's arms will create extra noise if the setup is not calibrated well enough before use. There are also a balanced homodyne method which can probe the phase fluctuations of graphene membrane. A laser Doppler vibrometry which uses optical interferometry, and, finally a Raman spectroscopy which can measure the dynamically induced strain in a membrane [23].

A transconductive readout is done by observing changes in the electrical resistance or conductance of the membrane with a setup such as one shown in Figure 2b. The method relies on a constant current I_d that flows through the 2D membrane. The resistance of the membrane is displacement-dependent $R(q_i)$, when the membrane moves, the voltage changes as $V_d = R(q_i)I_d \approx (R_0 + \frac{dR}{dq_i}q_i)I_d$. Where $\frac{dR}{dq_i}$ is the position dependence of the resistance. This derivative can be the result of the semiconducting nature of the material in a field-effect transistor geometry [23]. Another reason why the resistance changes is the piezoresistive effect. The effect happens when the membrane moves, therefore, changing the strain and lattice spacing in the membrane [23].

The capacitive readout method relies on an ac current flowing through a capacitor that is formed by the suspended membrane and the gate electrode a schematic can be seen in Fig-

ure 2c. This, yields in a time-dependent gate capacitance, $C_g(t) = \int_A \epsilon_0 dA/(g + w(x, y, t))$. Where A is the membrane area, g is much smaller than the membrane radius, and ϵ_0 is the permittivity of vacuum. When the membrane centre q_i changes the impedance of the capacitor changes accordingly $Z_C = 1/(i\omega C_g(q_i)) = V_{ac}/I_{ac}$ [23]. This method is hard to use in low frequencies because the capacitance has has tiny changes for a membrane that has a diameter that is a couple of micrometers. Therefore, the method typically used in the GHz range frequencies for a lower impedance [23].

A Mixed Readout with Capacitors and Transconductors is sometimes used since the high-frequency electrical signal from 2D membranes can be hard to detect. The high-impedance in the membrane causes a small motional signal and a large parasitic cross-talk from the driving voltage [23]. This makes it hard to distinguish between the signal and the noise in when they are at the same frequency. The problem can be solved by using a down-mixing scheme that changes the signal frequency to make it readable [23].

When down-mixing a transconductive signal, the membrane conductance G is modulated by the motion at a frequency ω_m and a modulated bias voltage V_{sd} at frequency ω_c. The two sinusoidal functions result in a low-frequency mixing term in the current I which is $\delta\omega = |\omega_c - \omega_m|$ [23].

A similar mixing technique is used for a capacitive radio-frequency (RF) signal. However, an electromagnetic wave's (EM) frequency ω_{EM} is now modulated by the motion of a mirror capacitor plate ata frequency ω_m. When a RF input at frequency ω_c is close to ω_{EM} is sent into an optical filter, it results in a mixed output signal $\omega_c \pm \omega_m$ [23].

A Position Dependenr Readout is done by using a localised probe such as a laser beam or an atomic force microscope which is shown in Figure 2d. The probe can measure $w(x, y, t_0)$ and compare it to $w(x, y, t_1)$ where $t_1 > t_0$. This is the only method that can measure the motion at one point. However, this method depends on the position of the probe, which means that it is good to have an idea of which mode the membrane is in when measuring before placing a probe [23].

1.1.3 Photonics

Photonics is the study of light and photons which started in 1960 with the invention of the laser [6]. Photonics have come a long way since the 1960s and and are an important part for modern society. Since they are used in telecommunications and sensors whether they detect photons, are used in cameras, detect in the infrared scale or for another application. This review will focus on a more recent development in photonics which involves silicon and creates the study of silicon photonics.

Silicon photonics uses silicon as a medium for the light wave whether it is in a transceiver or a waveguide. A waveguide is a thin strip of material that guides light (Electromagnetic waves or EM-waves), where a silicon waveguide typically transeives light around $1400nm$ to $1600nm$ [22]. The advantage of silicon with photonics is that silicon has a high refractive index contrast and silicon is very strong mechanically. Moreover, silicon devices can be made with existing Complementary metal–oxide–semiconductor (CMOS) fabrication technology [25].
The silicon photonic devices used for this study are silicon waveguides that consist of silicon dioxide (SiO_2) on the bottom, followed by silicon in the middle and air on the top. They are used to transceive any light coupled to the silicon in them. However, if the waveguide is designed without taking Snell's law, which explains the relationship between angle of refraction and incidence of light which is

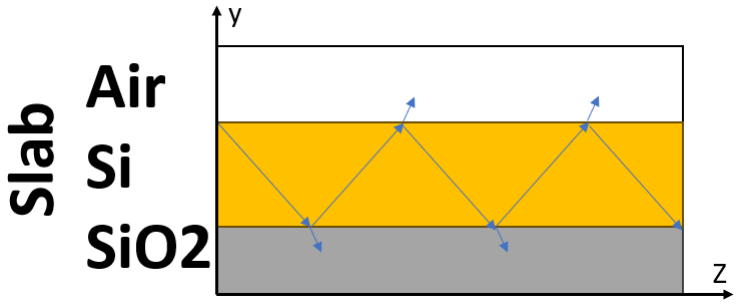

Figure 3: A waveguide slab showing the propagation of light.

$$n_1 \sin\theta_1 = n_2 \sin\theta_2 \tag{1.1}$$

where n_1 is the incident index, n_2 is the refractive index, θ_1 is the incident angle, and θ_2 is the refractive angle. For the light to be perfectly propagated by the waveguide, the light needs to have a critical angle of $\theta_2 = 90°$ on all sides of the waveguide as seen in Figure 3. In reality it is enough to be around the critical angle for the light to propagate through the guide. Although, the reflective angle is important the guide is actually designed around the effective group index (n_g) and the effective index (n_e). The effective index is calculated from the propagation constant (β) and the free-space propagation constant (k)

$$n_e \equiv \frac{\beta}{k}, \tag{1.2}$$

where the free-propagation constant is calculated from the free-space wavelength (λ) as $k = 2\pi/\lambda$. Calculating the the group index is done by taking the derivative of the effective index

$$n_g \equiv \frac{\delta\beta}{\delta k} = n_e - \lambda\frac{\delta n_e}{\delta\lambda}. \tag{1.3}$$

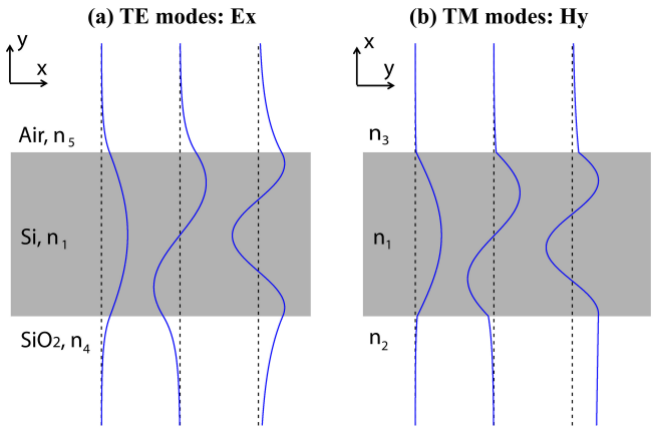

Figure 4: Transverse electric & transverse magnetic mode concentration in a waveguide. (Figure is taken from [25].)

Another important part of the waveguide is how the light propagates through it according to

$$\mathcal{E}(x,y,z,t) = E(x,y)e^{l(\omega t - \beta z)}, \tag{1.4}$$

where this equation describes the transverse electric (TE) mode propagating along the z-axis in time t, angular velocity ω, and amplitude $E(x,y)$. The transverse magnetic mode (TH) $\mathcal{H}(x,y,z,t)$ has an identical equation except E is replaced with H [25], [19]. Now since the

TE and TM modes are described in three-dimensions, there will be a different concentration of the fields depending on the x & y position of the waveguide. Where the TE field escapes the waveguide in all of its modes as seen in Figure 4.

Silicon waveguides are already in use as various detectors such as motion detectors at micro- or nanometre scale, a force sensor, or a thermal sensor [14], [12].

1.1.4 Two Dimensional Membranes with Photonic Waveguides

This method uses resonators in waveguides with 2D membranes placed on top to detect their motion. The motion is detected by observing a shift in the resonance dips that are caused by the resonators. In theory a shift is detected by comparing a resonance dip when the membrane is in position A versus the membrane in position B, Figure 5 is an example of how it would look like (The same method is used in opto-mechanical detection [14]).

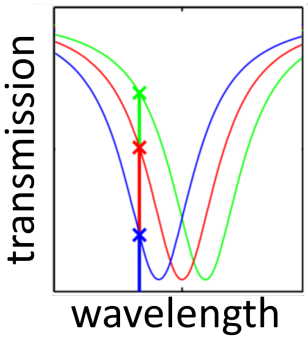

Figure 5: Comparison of resonance dips.

This method can in theory be used for sensors measuring as little as $7\mu m$ in width where the resonator measures $3\mu m$ in radius. However, waveguide resonators have not been tested with a 2D membrane on top of them. but they have been tested for carbon nanotubes [1]. Furthermore, there are theoretical papers on the subject that show cased a sensitivity of $28fm/\sqrt{Hz}$ with a Q-factor of 2400. The paper simulated a graphene membrane suspended over a ring that is integrated to a Mach-Zhedner interferometer [5]. However, there are no such devices used in this study therefore, the measured sensitivity can be assumed to be much greater than $28fm/\sqrt{Hz}$.

1.2 Project Proposal

Four different methods to detect motion in 2D membranes were discussed in subsubsection 1.1.2 and, a theoretical fifth method was proposed in subsubsection 1.1.4. Where the fifth method uses silicon photonics to measure changes in 2D membranes. However, because nobody has tried to measure 2D membrane mechanics with silicon photonics before, the question remains; can silicon photonics detect 2D membrane mechanics?

Silicon photonics can be used to make microscopic sensors which are easier to mass produce. Where optical readout methods often need a complex setup, transconductive and capacitive readouts are often down-mixed and a position dependent readout needs high accuracy when placing the probe [23]. The silicon photonics method will only need an input laser and a photodetector to measure an output signal.

The problem can be solved by doing experiments with the proposed detection method. The

experiments would be conducted by using a SOI test chip that has many different waveguide resonators built in it. The chip would be placed in a setup that is connected to a laser and a photoreceiver. The goal is to successfully measure 2D membrane motion with silicon photonics.

2 Methods

The methodology of fabricating a suitable 2D membrane and then measuring said membrane is discussed here. The section starts by going over the different stages of the fabrication process and why a new transferring method was used instead of using a well known method. The second part of the section describes how the membrane is measured and what precautions are made to confirm the results. The annealing setup is shown and explained in Appendix A

2.1 2D membrane Transfer

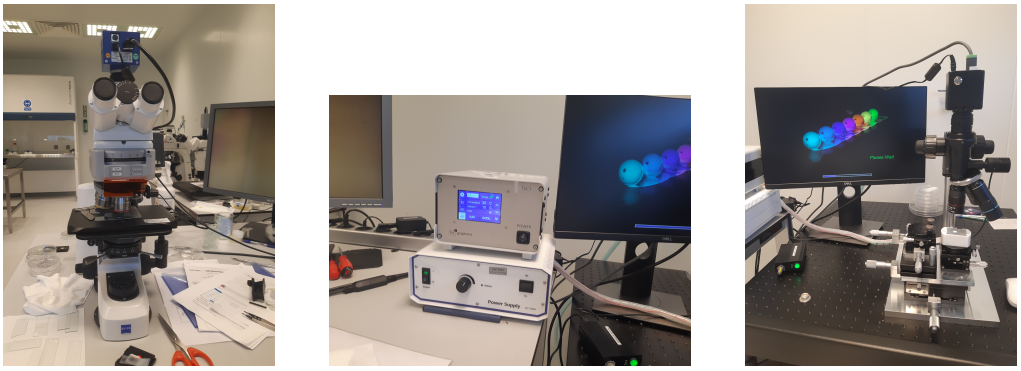

(a) (b) (c)

Figure 6

Figure 7: The Graphene transfer setup. This setup is used to transfer the 2D membranes to the SOI chip, figure a) shows the microscope where suitable flakes are found, the lower box in figure b) is the light intensity controller for the microscope and the upper box is the vacuum and temperature controller for the transfer setup, which is shown in figure c) with its light intensity controller to the left.

This section is split into two parts. The first part talks about the 2D membrane transfer method that was used in the literature review and mentions. The second part goes over a new transfer method that is used for this thesis. This subsection ends by going over the advantages and disadvantages of both methods and some of the achievements that were made.

2.1.1 Old 2D membrane Transfer Method

When transferring a membrane on top of an SOI chip, a 2D membrane is needed. A simple way to get a 2D membrane, is by sandwiching it between two strips of tape and ripping the two parts from each other. This step will will only make the membrane sample thinner and the step has to be repeated multiple times by sandwiching a clean tape with one that has graphite on it. After the process has been repeated at least three times it is possible to confirm the results by putting the tape under a microscope. This step is not needed for the whole process, however, it can ensure that there are 2D membranes on the tape. When the membrane is thin enough it is possible to press Polydimethylsiloxane (PDMS) (which is a sticky polymer) to the tape with the membrane flakes and rip the PDMS from it. After this is done it is good to put the PDMS under a microscope to make sure that there is some 2D membrane on the polymer. The membrane that is two dimensional should look transparent on top of the silicon. The PDMS is then finally aligned with the chip to put a desirable 2D membrane flake on top of a resonator (this is done under a microscope). The PDMS is pressed up to the SOI chip until the flake is touching the chip, the PDMS is then slowly pulled from the chip to make sure that the 2D membrane holds on to the SOI and not the PDMS. This step can be repeated if the flake does not stick to the

chip at first and changing the temperature may help.

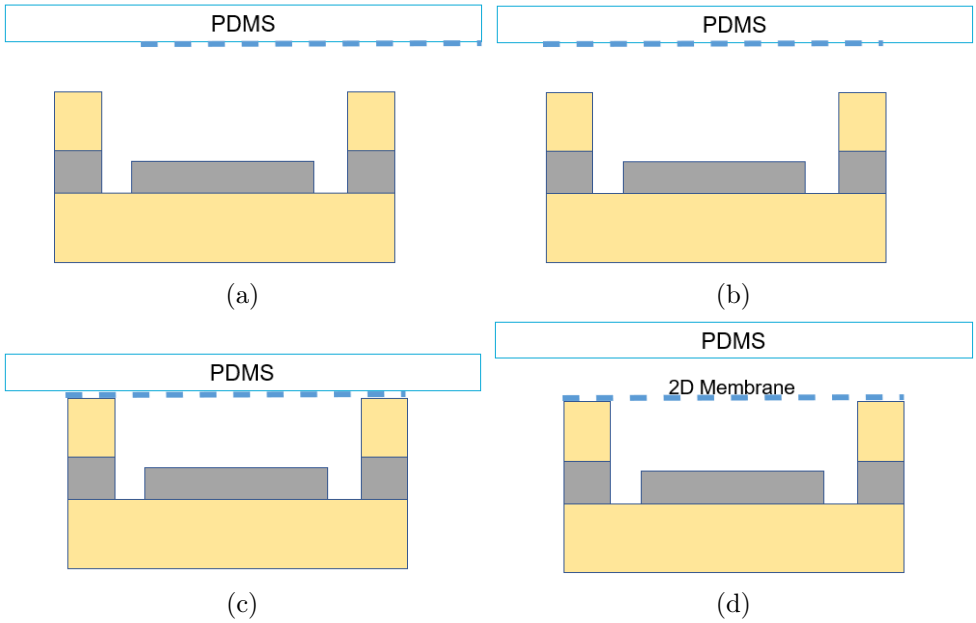

Figure 8: Here are the steps for transferring 2D membrane, where figure a) shows the alignment step. Figure b) shows the 2D membrane aligned and ready to be transferred. Figure c) the 2D membrane is touching the SOI chip and in figure d) the 2D membrane has been successfully transferred on the SOI chip.

2.1.2 New 2D membrane Transfer Method

The new 2D membrane transfer method developed by Niels Bouman and is based on a method used by Kei Kinoshita et al [9] uses a layer of polypropylene (PPC) to transfer the 2D membrane. However, before transferring the 2D membrane, a film of PPC is fabricated. The fabrication starts with a PPC solution that consists of 15% PPC and 85% anisole. A pipette is used to place a small drop ($> 1ml$) on a thin square coverslip ($25mm \times 25mm$). The slide is then placed in a spinner to spread the PPC to form a thin film. After the PPC has cured over two days at room temperature, the PPC film is ready for use. The film is then peeled of the slide by using tape that covers the slide´s edges therefore, forming a square gap in the center for the film to stretch over a PDMS dome. A sharp knife or a scalpel is slid under a corner of the tape square to peel the film of its sheet. After the film has been successfully peeled of the sheet, the film is placed on top of a PDMS dome that sits on a microscope slide ($26mm \times 75mm$) as seen in Figure 10.

After the preparation for the PPC stamp is done, the 2D membrane can finally be transferred to a PDMS sheet similarly to the old method. However, that is where most of the methods similarities end. Now, instead of transferring the membrane directly onto a chip, we transfer the membrane to the PPC stamp. The stamp is then aligned over a suitable device on the SOI chip. After the 2D membrane is in position above a device, the dome is lowered until the membrane hangs comfortably above the device. The device is then heated up to $120°C$, this melts the PPC which becomes a very viscous fluid. The stamp can be removed when the PPC has stopped expanding and reached a stable state. However, this is a very dirty process and can leave a this layer of PPC over a large area ($R \approx 300\ \mu m$), the transfer process is shown in Figure 9. The

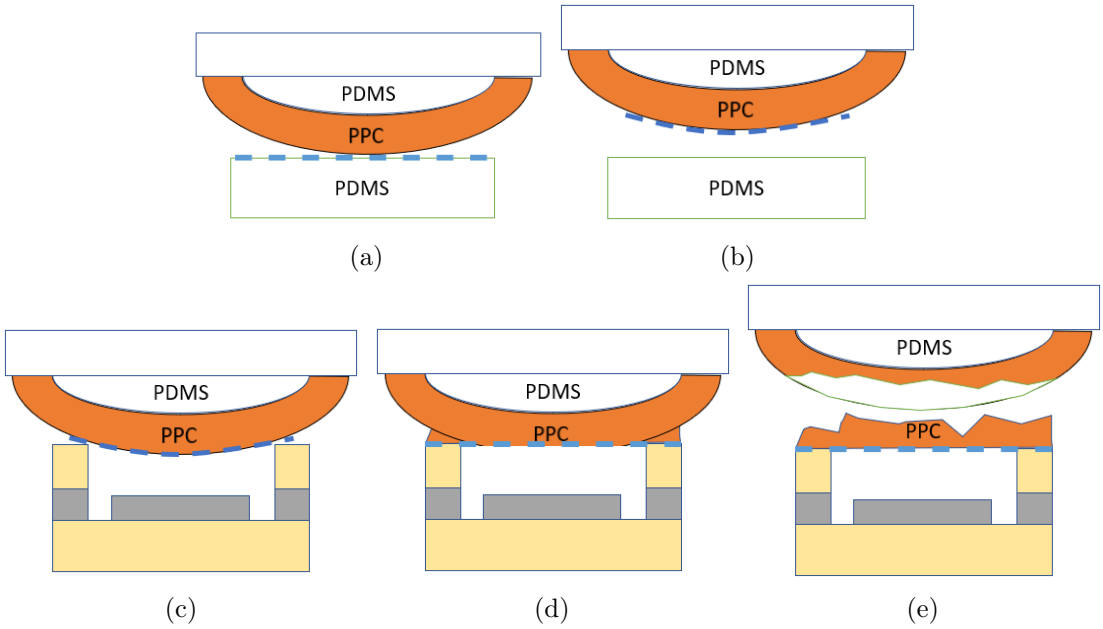

Figure 9: The new transfer method is shown here, where figures a) & b) show a graphene being transferred from a PDMS sheet to a PPC covered dome. Figure c) the graphene is touching the SOI chip before the PPC is heated to 120 °C which is done in figure d). In figure e) the graphene, and a small layer of PPC, has been successfully transferred on the SOI chip.

final step of the process is to remove any PPC residue that is on the chip.

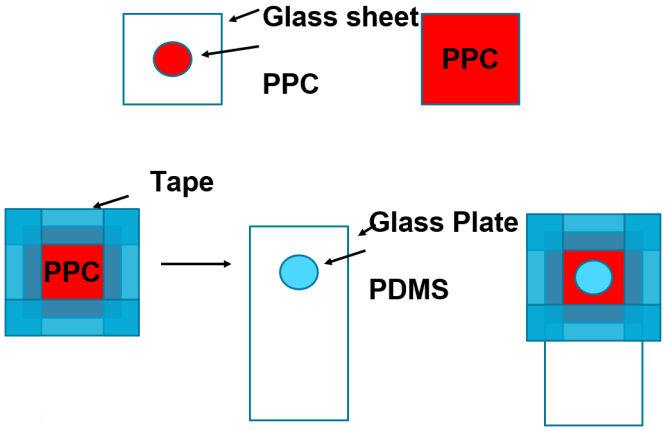

Figure 10: The PPC film preparation is shown here. First a drop of PPC is placed on a glass slide, the slide is spun and coated by the PPC. After a PPC film has formed and cured it is peeled of the slide and placed on top of a PDMS dome.

The post-processing consists of putting the chip through an annealing process in order to remove the PPC layer of off the chip. The chip is put into a high vacuum chamber ($> 10^{-5}$ mbar) that is heated up to $400°C$ and is left there for two hours before the chamber is cooled for at least eight hours before the chip is removed. This method was used to transfer all graphene samples to the chip.

2.1.3 Comparison

The old transfer method is a fast method, since it takes only about an hour to transfer a membrane flake. Compare that to the new transfer method which adds at least ten hours for every successful transferring session with a minimum of eight hours of downtime due to annealing. It is easy to see that the old method is superior with respect to time. However, the old method also covers most of the chip when a membrane is transferred. This can lead to undesirable membranes covering excellent devices. Therefore, limiting potential resonators on a chip. The new method addresses this issue by using a dome shaped stamp. By using a dome, the contact radius between the chip and the stamp decreases to below a radius of $200\mu m$. Thus allowing for more membrane transfers for a single chip. In conclusion, due to the importance of being able to test many devices, the new method was chosen for all transfers in this thesis.

2.1.4 A Mixed Method

Due to multiple devices breaking between graphene transfers that used the new method and, a single dry transfer made on the chip, it was decided that a mixture of Bouman's and Kinoshita's method was used. This method uses the same methodology as Bouman's method, however, instead of melting the PPC thus ensuring the transfer, the PPC is heated to $70°C$ which makes the PPC's grip on the membrane weaker.

2.2 Measurement Setups

The chip's measurements consists of sensing the 2D membrane and mapping the topography of the chip. Furthermore, each device on the chip is measured at least once, the first measurement is done before membrane transfer and gives the device's transmission which shows whether the device is suitable for a membrane transfer. The second measurement is done after the transfer which makes for an easy comparison of the data before and after membrane transfer. After the chip measurements are complete, the membrane is measured with a laser interferometer. The data from the interferometer is mainly used to compare and confirm the results from the silicon photonic setup. However, the interferometer will also make it clear whether or not the membrane is truly suspended over its device. The final measurement is the topology mapping. The chip's topology is sensed with both an atomic force microscope and a white light intereferometer.

2.2.1 Silicon Photonics setup

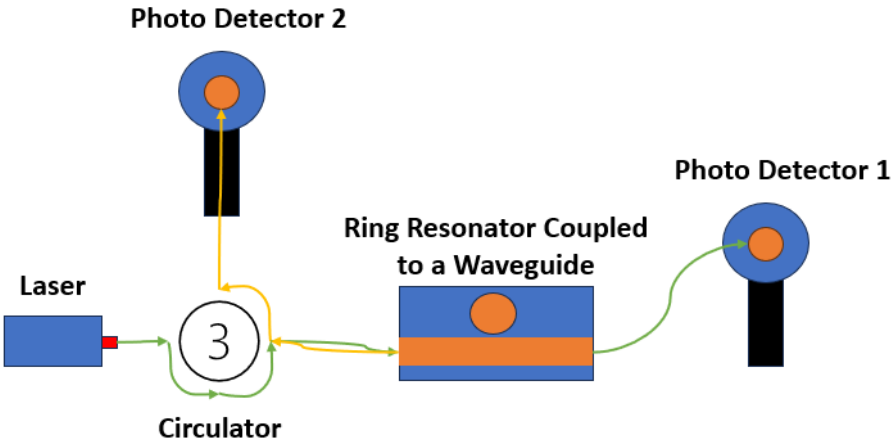

Figure 11: The Silicon Photonic Setup is shown here with a circulator (with three ports) that guides any reflected laser to an alternative photo detector.

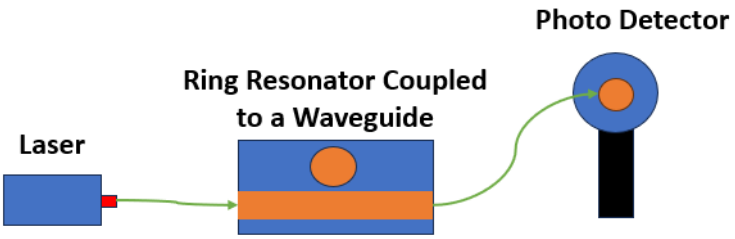

Figure 12: The Silicon Photonic Setup without a circulator is shown here.

The silicon photonic setup is used to measure 2D membrane's motion with a silicon waveguide resonator. This setup relies on a photodetector, that reads the laser signal after it has gone through the waveguide resonator. Other parts for the setup are either a $3dB$ attenuator or a $10dB$ attenuator, a circulator , and a second photodetector, the optic schematics are shown in Figure 11. The setup's attenuator is used to limit the $10dBm$ laser power, therefore, keeping the chip and measurement devices save from potential damage. While, the circulator is attached to the second photodetector, therefore, measuring the internal reflection of the waveguide. The internal reflection can help give understanding if a membrane over a specific silicon device, is absorbing the laser or not.

Furthermore, this setup can be used to measure a DC signal while sweeping over the laser's wavelength range ($1530nm \leq \lambda \leq 1620nm$). The laser has a sweeping range of $50nm/s$ and power of $10dBm$. The output signal shows the corresponding device transmission when the laser is swept in such a way. In case of acceptable devices, the transmission will show a steep resonance dip close to the maximum transmission signal. This dip or more accurately the lower flank of the dip is used to measure AC signal at a single wavelength. The whole flank is measured with a wavelength step of $\Delta\lambda 0.01nm$ with a time length (t) of $200\mu s$. This is done to ensure a near full coverage of the resonance dip's flank. The AC signal is then converted to the frequency domain with a fast Fourier transform algorithm.

This setup allows for a simple way to measure the SOI chip. However, to measure the membrane mechanics, the membrane needs to be actuated for it to have any influence on the transmission signal. One way to actuate the membrane is to modulate the laser that shines upon it. There are two ways to modulate the laser, either by using an electro-optic modulator or an acousto-optic modulator. The other actuation method uses a piezo shaker that will actuate the entire chip. The biggest downside of actuating the whole chip is that it is harder to couple the laser to the waveguide.

2.2.2 Laser Interferometry

The laser interferometry measurements rely on two lasers pointed at the 2D membrane, one actuates the membrane while the other one measures its motion as seen in Figure 13. Since the method is based on two different principles this section is split into two parts, and will first look into the measuring part.

Laser interferometry measurement was briefly discussed in subsubsection 1.1.2 and, will go into more details here since it is used as a control measurement. The membrane motion is measured by shining a red Helium-Neon laser ($\lambda = 632.8$nm) at the suspended 2D membrane. Since 2D membrane is an atomically thin reflective material, some of the laser bounces of off the membrane (L_0) while a part of it shines through the 2D membrane(L_G). When the laser shines through the 2D membrane it is reflected from the back-plate and back through the 2D

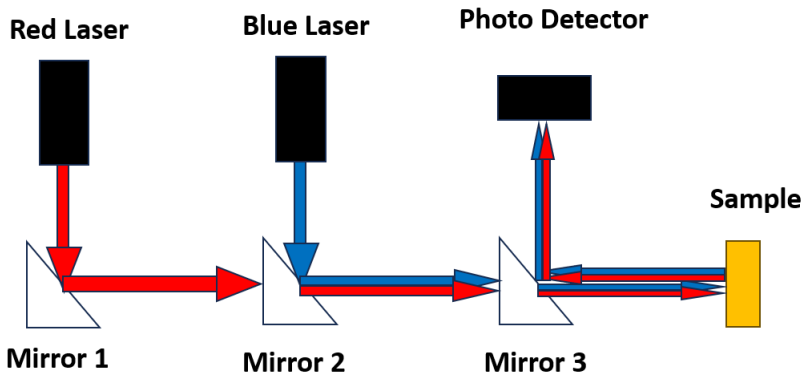

Figure 13: The laser interferometer is shown here where a red laser ($\lambda = 632.8nm$) is used to detect the membranes motion and a blue laser ($\lambda = 405nm$) is used to actuate the membrane.

membrane. The time delay from the extra distance to the back-plate and back through the 2D membrane causes a phase shift in the reflected laser. The merge between L_G and L_0 causes an interference between the two lasers, the resulting strength of the laser can detect the motion and frequency of the membrane. The membrane is excited by a blue laser ($\lambda = 405$nm).

2.3 Chip's Topography

Although, the motion measurements are the focus of this research, it is still important to map the topography of the 2D membrane. The topography is mapped with an atomic force microscope (AFM) and a white light interferometer (WLI). The AFM measures the chip by moving a cantilever along the chip's surface. This allows the AFM the gather the positional data from its cantilever and create a topological image of the chip. Assuming that the cantilever does not break the 2D membrane, the AFM is able to measure the membrane thickness and how much the membrane sags over its cavity.

The WLI works in the same way as the laser interferometer, however, instead of using a laser that can actuate the 2D membrane, the WLI uses a neutral light that shines through a Fabry-Pértot interferometer to create an interference in the reflected light.

2.4 Working with Raw Data

The data collected from the discussed methods comes out as raw data. Most if not all of the data needs to be converted into meaningful units before the data gives any meaningful results. This can be either from amplifiers in the measuring setup or due to excessive amount of noise in one domain compared to another, e.g., conversion between the time domain and the frequency domain.

2.4.1 Silicon Photonic Data

There are three types of data from the silicon photonic setup. The main data comes from the laser that propagated through the waveguide and beamed out of the opposite end. This is the waveguide's transmission signal, which does not need to be heavily edited. This is due to the transmission itself being the important part of the data. After the transmission signal has been recorded, it is possible to measure the AC signal of the transmission. Unlike the first data set, this one needs to be converted from the time domain and in to the frequency domain. However it is not needed to calculate the power of the AC signal, due to the frequency values being the more important factor of this signal. The final data is due to internal reflections of the

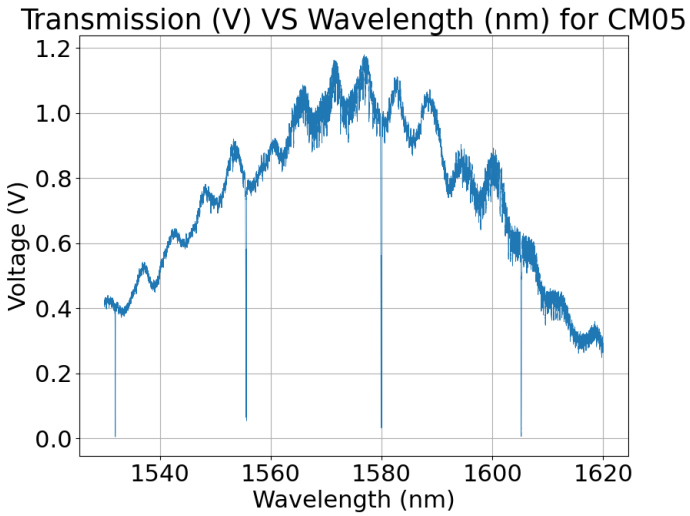

Figure 14: Transmission graph of a device that has a $10\mu m$ radius cavity with a ring radius of $4\mu m$, a coupling gap of $0.25\mu m$, and a waveguide height of $0.15\mu m$.

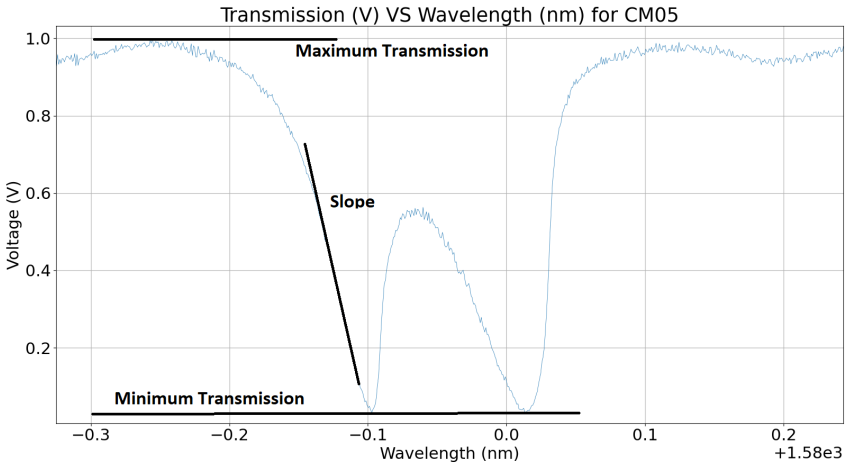

Figure 15: A close up of a resonance dip with reference lines.

waveguide. Therefore, it is measured with a different photo detector compared to the other two signals. The new detector uses an amplifier to strengthen the signal, thus making it necessary to either convert the data in to correct units or normalize the data. This is done because the amplification for the detector is changed manually which can lead to two different data sets having identical data, but, different magnification.

The transmission signal is measured in volts that sweeps over the wavelengths $1530nm$ to $1620nm$ at a rate of $50nm/s$. The input power was $10dBm$ with a $3dB$ attenuator for die1 and a $10dB$ attenuator for die2. A typical device on the chip shows maximum transmission power between $1560nm$ to $1580nm$. Furthermore, due to the coupled resonators there will be resonance dips when looking at a graph of transmission versus wavelength such as Figure 14. These resonance dips are the most important part of the transmission signal where a closeup of such a dip can be seen in Figure 15. The important bits of the resonance dip are its left flank, the flank's slope and the flank's extinction ratio (e_{ratio}). The ratio is calculated with

$$e_{ratio} = \frac{T_{min}}{T_{max}} \tag{2.1}$$

where T_{min} is the minimum transmission of the resonance dip and T_{max} is the maximum transmission of the dip. A low ratio should result in a steep slope (s) which is the derivative of the transmission over the wavelength

$$s = \frac{\delta T}{\delta \lambda}. \tag{2.2}$$

This leads to a final variable, the total sensitivity (S), which is used to determine whether a device is good or not.

$$S = s \times \frac{W_b}{W_0} \tag{2.3}$$

The total sensitivity stems from the slope multiplied by the maximum position of the membrane over the waveguide (W_b) versus the membrane's maximum position at its center (W_0).

The AC current is measured by fixing the laser's wavelength to the left flank of a resonance dip. The flank can either be confirmed by manually changing the wavelength and seeing how the dc signal changes through an oscilloscope or by sweeping the laser over the expected flank wavelengths and seeing how the dc signal changes. The wavelength is then fixed after the flank has been confirmed and the AC signal is measured for $200\mu s$. The data is then used to determine the natural frequency of each device or in the very least if there are any resonating modes in the expected range of the natural frequency of 2D membranes. The AC signal is converted from the time domain and into the frequency domain with a fast Fourier transformation. When a 2D membrane is on top of a device. It is possible to determine the motion of the membrane from its frequency via

$$m_i \ddot{q}_i + c_i \dot{q}_i + k_i(q_i - q_b) = 0 \tag{2.4}$$

where m_i is the membrane mass, c_i is the damping coefficient of the membrane, k_i is the membrane stiffness, and q is the membrane's position. Furthermore, the air that is trapped under the 2D membrane will influence c_i and k_i due to the squeeze film effect [18], [15].

The reflected signal is normalized to make comparison between the signal before and after membrane transfer easier.

3 Results

The section starts with going over the graphene transfer which showcases the used devices. Then the measurements from the silicon photonics setup are shown. Next are the results with a graphene membrane, including laser interferometry results. The interferometry results are to confirm that the graphene is indeed suspended over a resonating device. After the graphene measurements, results with MoS_2 are shown. These results will also show why MoS_2 is preferred over graphene. The section finishes off with topology measurements.

3.1 Membrane Transfer

Both the new transfer method (subsubsection 2.1.2) and the mixed transfer method (subsubsection 2.1.4) were in general very successful where the new method was used on die1 and the mixed method was used on die2.

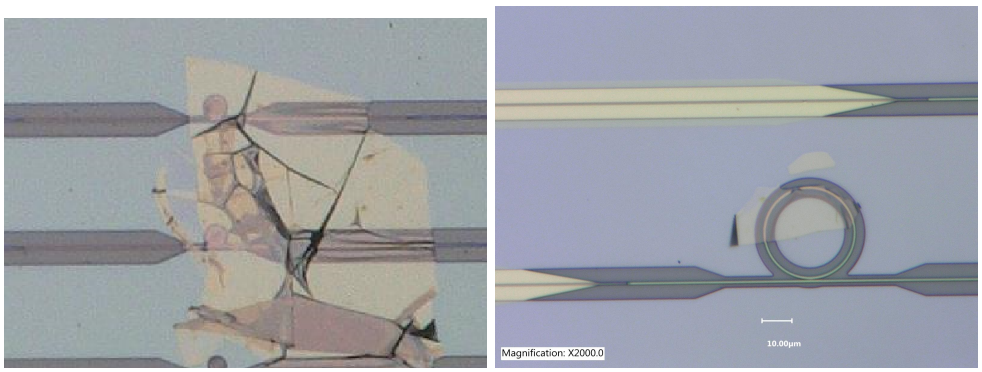

(a) (b)

Figure 16: The graphene transfer on die1. a) shows a large flake covering multiple circular membrane devices, b) shows a smaller flake covering a doughnut membrane device.

The transfers shown in Figure 16 & Figure 17 seem to have larger flakes when it comes to the CM devices. The reason is that the CM devices are much smaller than the DM devices which makes the CM flakes seem larger in comparison when, the flakes are in fact of similar sizes.

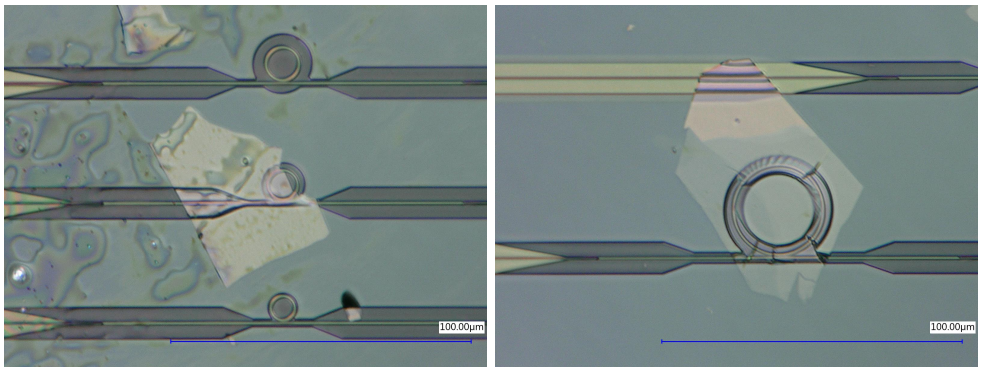

(a) (b)

Figure 17: The MoS_2 transfer on die2. a) The membrane on top of the CM device looks dirty because of a contamination on the stamp before the membrane was transferred. b) The membrane suspended over the DM device was transferred without any problems.

3.2 Silicon Photonics Without a Membrane

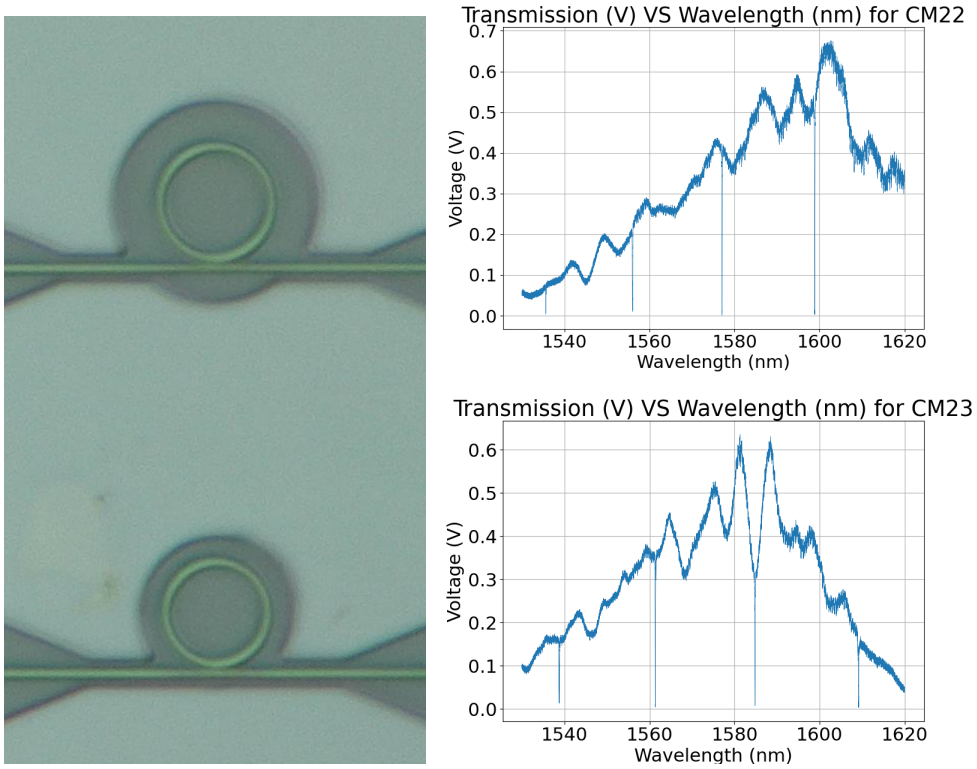

(a) (b)

Figure 18: An example of two different circular membrane devices with their respective transmission over wavelength graphs.

The results from silicon photonic measurements look promising. The acquired data suggests there are many different devices that can be used, e.g., the circular membrane devices shown in Figure 18. However, as the chip was measured again and again, some devices started to show cracks in them which decreased the amount of devices suitable for 2D membrane transfers. Therefore, it was decided to change from circular membrane (CM) devices to doughnut membrane (DM) devices, see Figure 19.

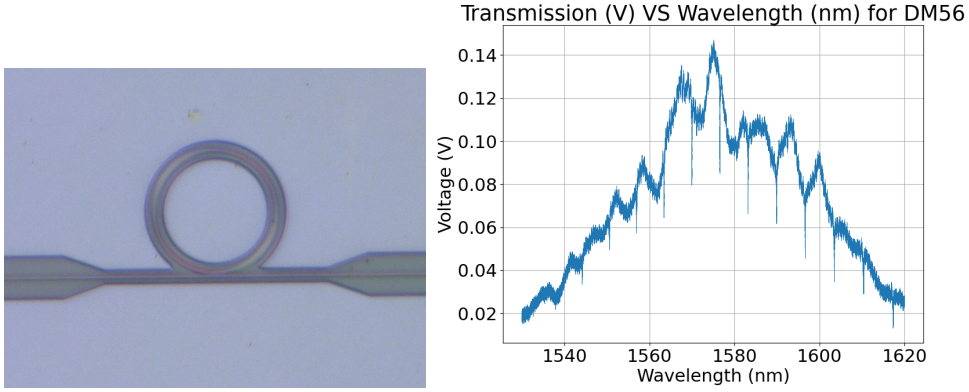

(a) (b)

Figure 19: An example of a DM device with its transmission and reflection over wavelength graphs.

The AC measurements results are converted in to the frequency domain which shows that neither the setup and the ring resonator are resonating in the range of interest as seen in Figure 26.

The normalized reflection data for a DM device with a coupling gap of $0.3\mu m$, a trench width of $3\mu m$, and a waveguide height of $0.1\mu m$ (DM71) shows that there is little reflection coming back from the device as seen in Figure 20. This device is used for the graphene transfer and comes from die1. The MoS_2 transfer uses an identical device from die2. However, due to the MoS_2 being on a new die, a separate reflection graph is used and is seen in Figure 21.

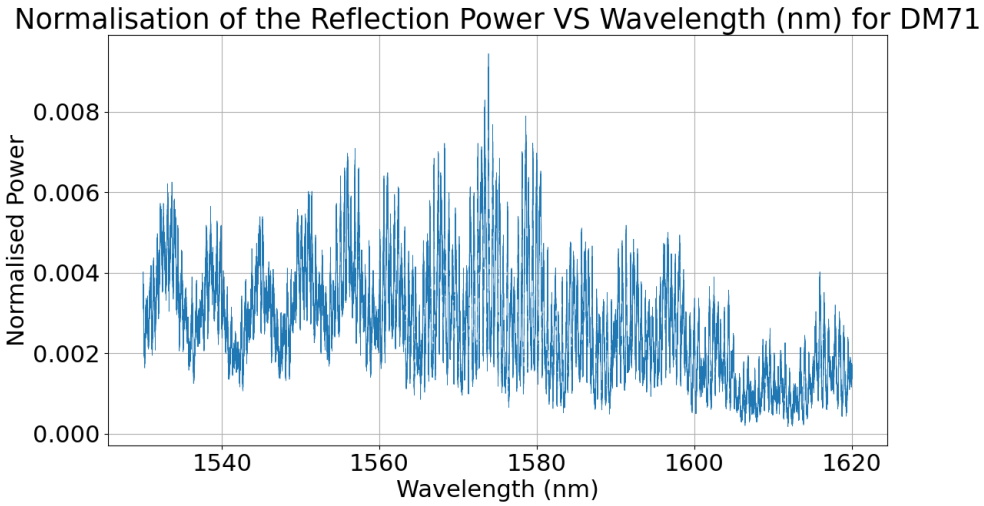

Figure 20: The normalized reflection for DM71 on Die1

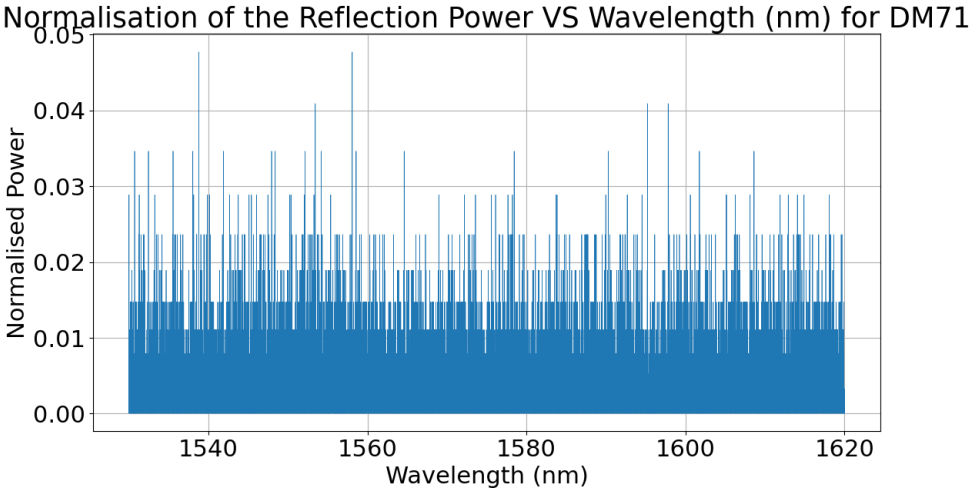

Figure 21: The normalized reflection for DM71 on Die2

DM71 was chosen on die2 due to its promising transmission graph and, there is a bad performing device between DM71 and the next promising device. While DM71 on die1 was chosen due to it being one of the last working devices on the chip.

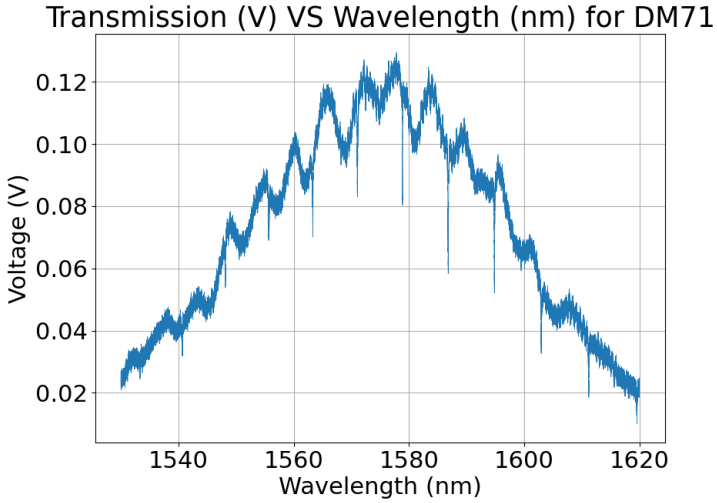

Figure 22: The transmission for DM71 on Die1 with an input power of $10dBm$ and a $3dB$ attenuator.

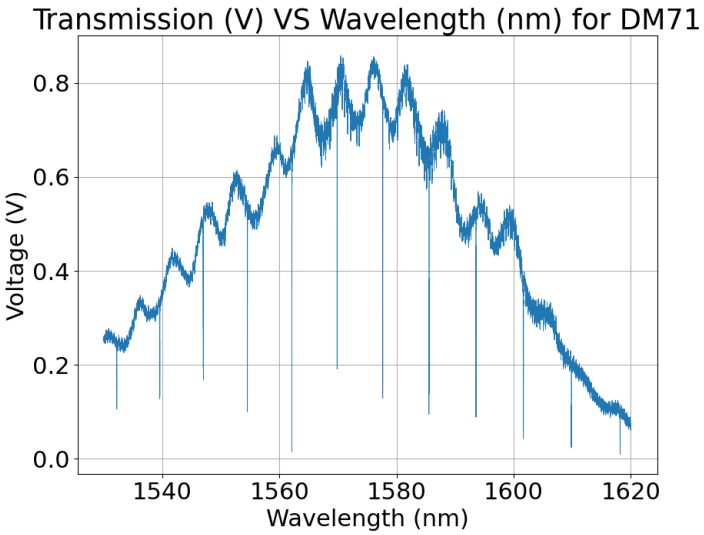

Figure 23: The transmission for DM71 on Die2 with an input power of $10dBm$ and a $10dB$ attenuator.

Die1 and die2 have a large difference in their performance and thus their flank wavelength is at different wavelengths which can be confirmed when comparing Figure 22 and Figure 23. The device on die1 is measured at a wavelength close to $1580nm$ while the wavelength for die2 is a bit larger than $1560nm$. However, the resulting AC-signals are quite similar to each other despite the difference in transmission.

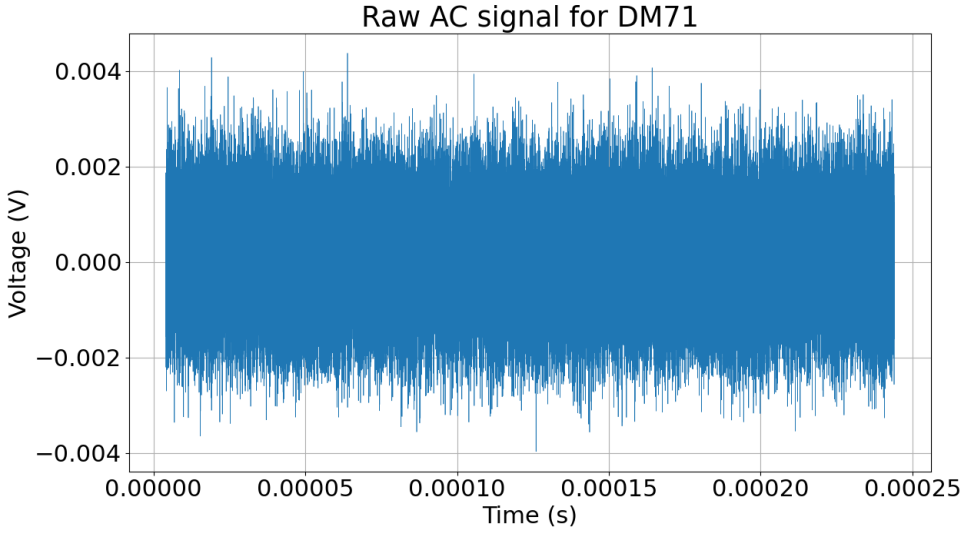

Figure 24: The AC-signal for DM71 on Die1 with an input power of $10dBm$ and a $3dB$ attenuator.

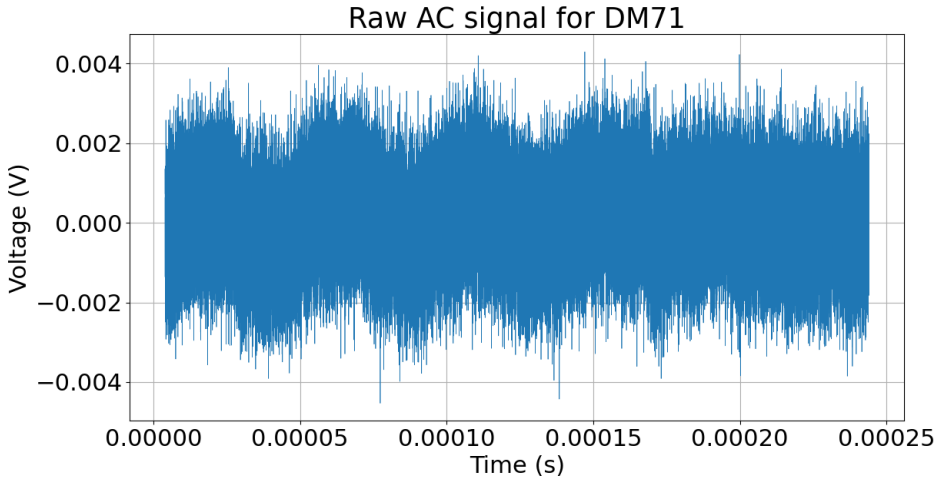

Figure 25: The AC-signal for DM71 on Die2 with an input power of $10dBm$ and a $10dB$ attenuator.

This similarity leads to near identical graphs in the frequency domain after a FFT.

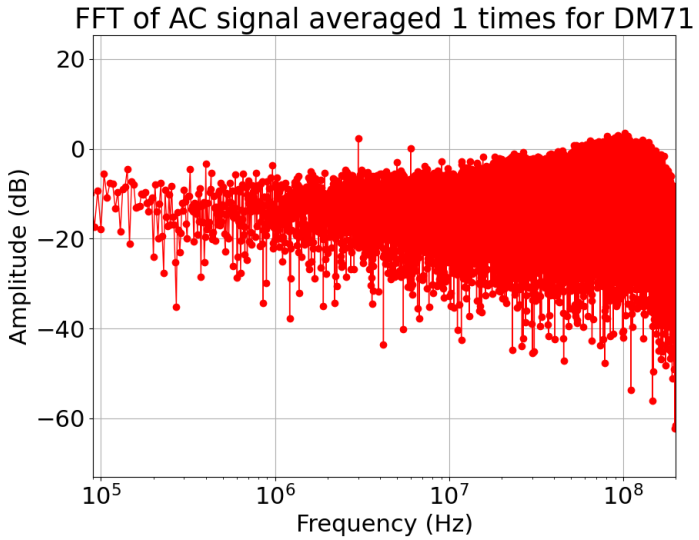

Figure 26: The frequency domain for DM71 on Die1 with an input power of $10dBm$ and a $3dB$ attenuator.

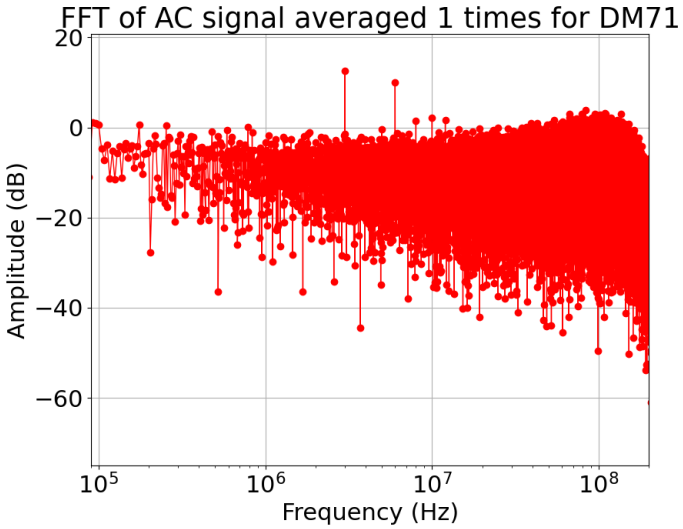

Figure 27: The frequency domain for DM71 on Die2 with an input power of $10dBm$ and a $10dB$ attenuator.

The frequency domain for DM71 on both dies shows a peak at $3MHz$ that consists of a single point. There is also a visible single pointed peak at $6MHz$ for the device on die2. Since these peaks consist of only a single point, they should not interfere with the natural frequency of a membrain laid over the devices.

These measurements wee also done for a device with a ring radius of $5\mu m$, a membrane radius of $7.5\mu m$, and a coupling gap of $0.3\mu m$ (CM23).

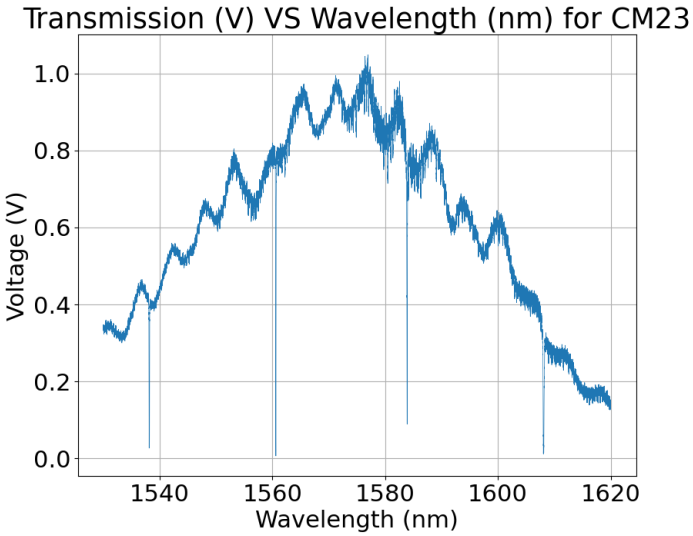

Figure 28: Transmission graph for CM23

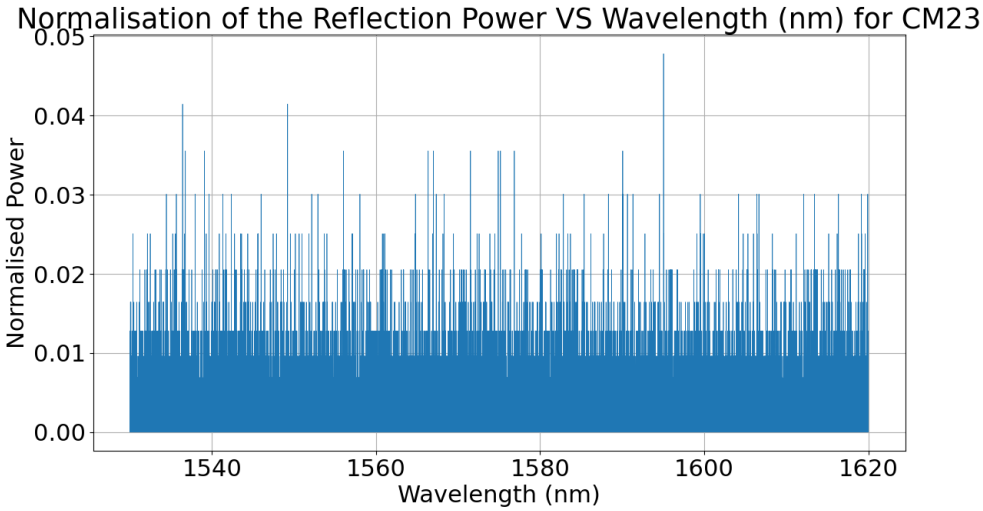

Figure 29: Reflection graph for CM23

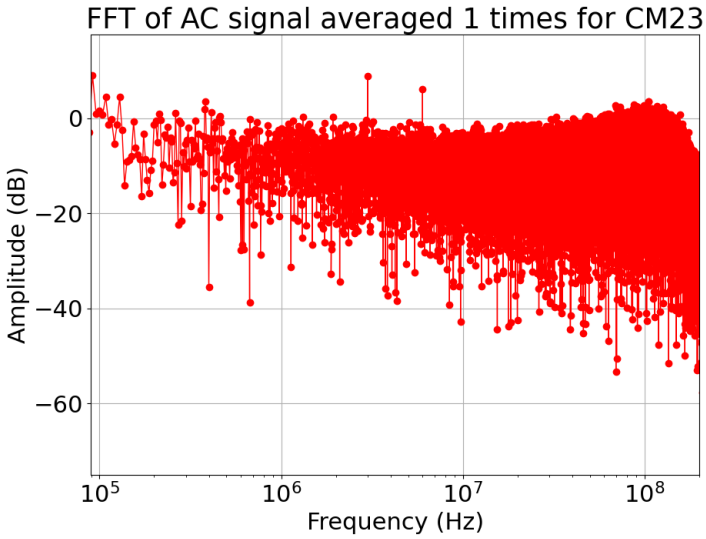

Figure 30: Frequency domain for CM23

The results from CM23 shown in Figure 28 to Figure 30 show that there is little to no difference between CM and DM when it comes to sensing 2D membranes.

3.3 Graphene Results

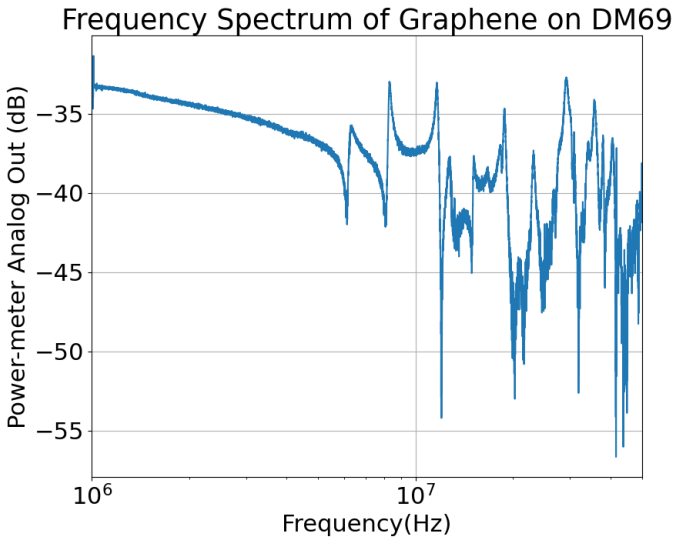

Figure 31: Frequency domain of a graphene membrane over a doughnut membrane device when measured with a laser interferometer.

The laser interferometer results with a graphene membrane confirmed that the fabricated graphene membranes have a natural frequency around $10MHz$ which is the recorded natural frequency [8].

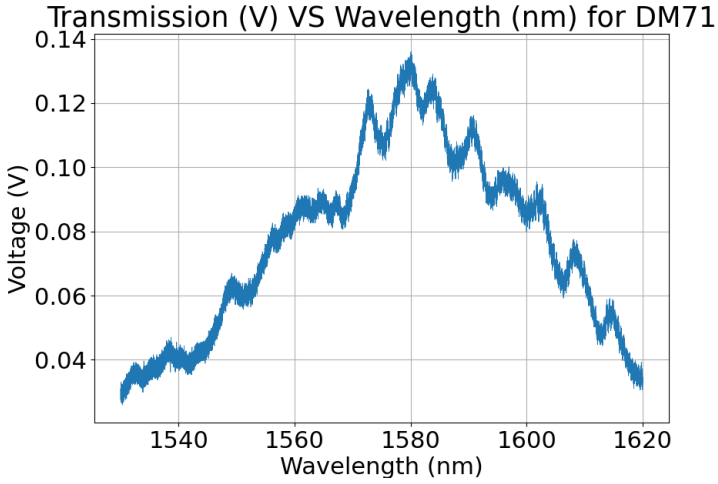

Figure 32: Transmission power for device DM71 after graphene transfer

The silicon photonic results were less promising after the devices were covered with a graphene membrane. The data shows a high decrease in transmitted power when the graphene covers the straight waveguide, and when the graphene is only covering the ring resonator (as seen on DM71 in Figure 16b), the transmission loses its resonance dips. Therefore, there were no flank measurements made with the graphene covered devices.

The data from the laser reflection hints that the graphene is either absorbing or scattering

most of the laser instead of reflecting it. Therefore, hindering an excellent propagation through the guide. This can be confirmed by comparing the normalized reflection before and after the graphene transfer, seen in Figure 20 and Figure 33 which shows $\sim 84\%$ decrease in reflection power at $\lambda = 1560nm$.

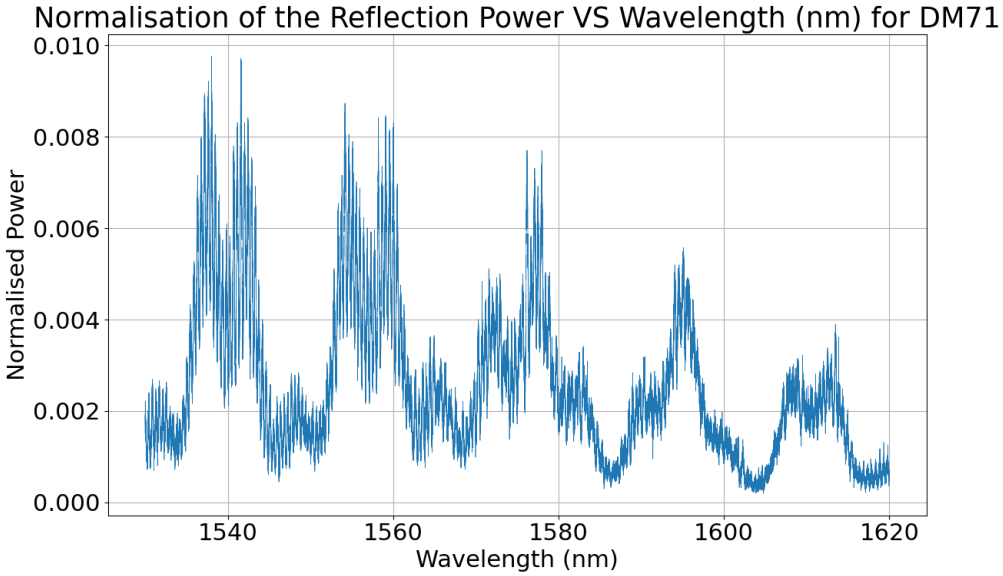

Figure 33: Reflection of DM71 after graphene transfer

3.4 Molybdenum Disulfide (MoS_2) Results

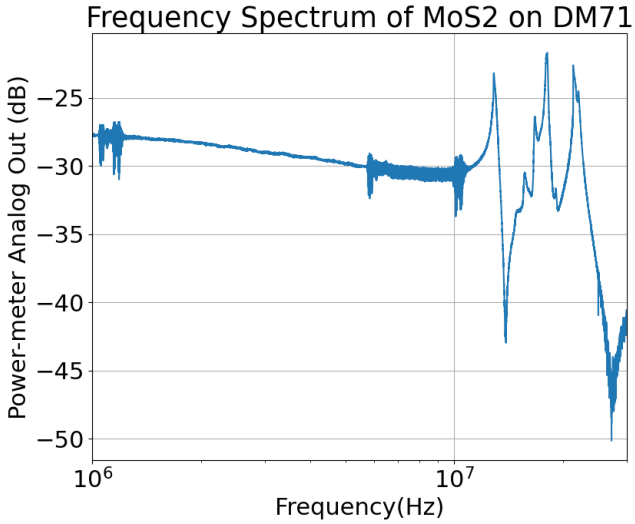

Figure 34: The frequency response for device DM71 on die2 when measured with a laser interferometer.

The Laser interferometry measurements for the MoS_2 membrane confirms that its natural frequency is between $1MHz$ and $10MHz$.

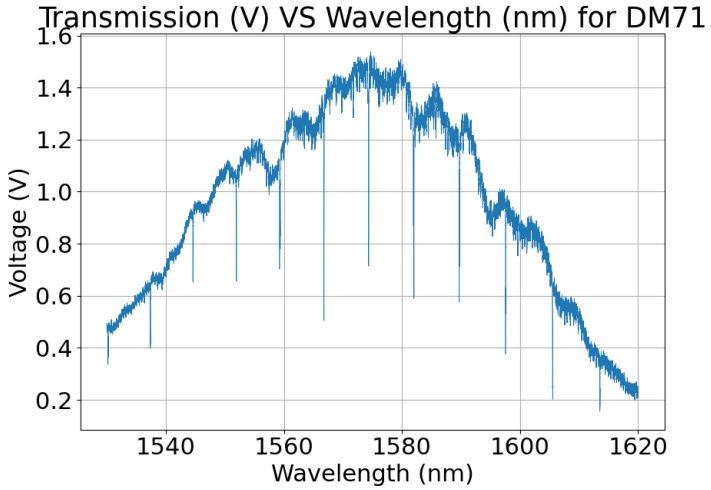

Figure 35: Transmission of device DM71 after MoS_2 transfer.

The results from the silicon photonics measurements look very promising. The first thing that the data shows, is that there are still clear resonance dips when looking at the transmission as seen in **??**. Furthermore, because the dips are present, it is possible to measure the AC signal over the dip's left flank. The data from the AC measurements need to be converted in to the frequency domain, which can tell if the membrane is resonating. **??**

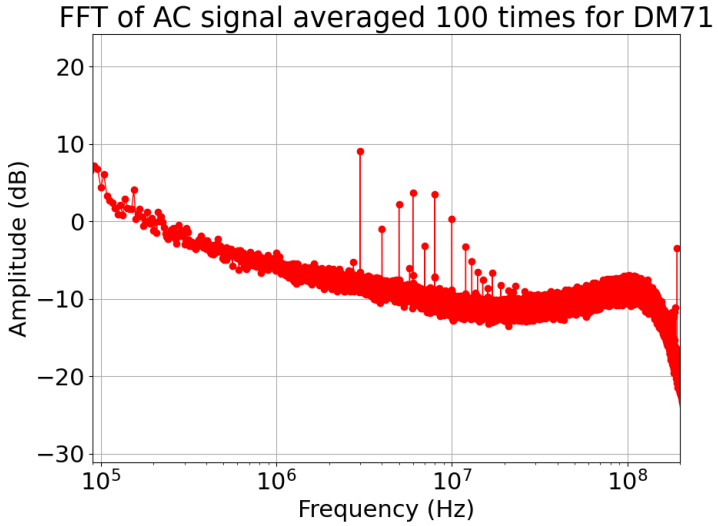

Figure 36: The Fourier transformation for DM71 at the resonance flank averaged one thousand times.

The frequency domain for device DM71 shows a clear resonance at exactly 3MHz and a few minor resonances at higher frequencies. However, the same peaks appear on other devices both before and after transfer, i.e., the signal is either due to the ring itself detecting an outside signal or the peaks are caused internally in the detection setup. To find out if the peaks come from the setup; the flank for device CM23 & DM71 was measured thousand times and then averaged as seen in Figure 38 & **??**. These two graphs show that the single point peaks are in the same position as Figure 27 & Figure 30. The peaks are also clearly made out of a single point in the graph. This hints to the peaks to be a result of the setup, i.e. the peaks are most probably due

to the electrical signals to the oscilloscope.

Thankfully, when making comparisons for the reflection data before and after MoS_2 transfer as seen in Figure 21 and Figure 37, the signal seems to increase. Which means that a part of the transmission losses are due to reflection.

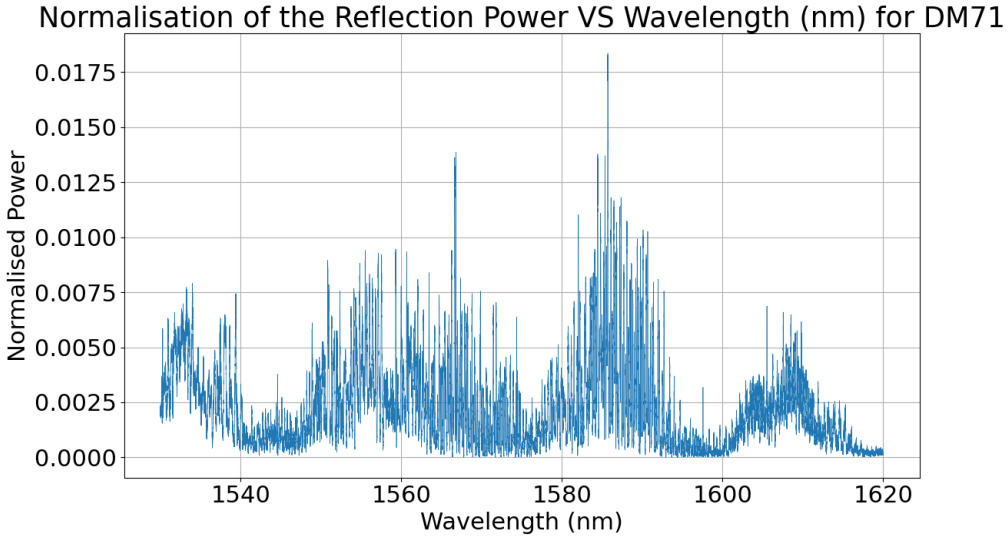

Figure 37: The normalized reflection for DM71 on Die2 after MoS_2 transfer.

The measurements were also done for CM23 which has a similar story, thus only showing the frequency domain of the AC-signal.

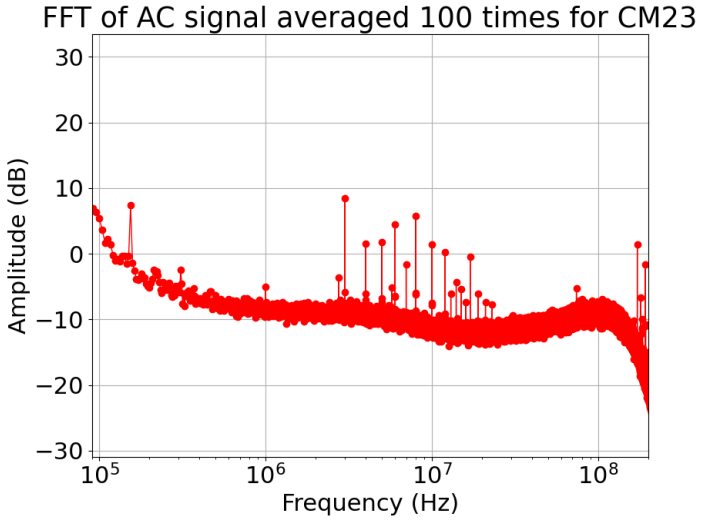

Figure 38: The Fourier transformation for CM23 at the resonance flank averaged one thousand times.

3.5 Topography measurements

The topography results are different between the AFM and the white light interferometer. Where the AFM gives a more accurate measurement which is confirmed in Figure 39. The waveguide

that was measured sits in a row of waveguides that measure $100nm$ in height which is $20nm$ of from the measured height.

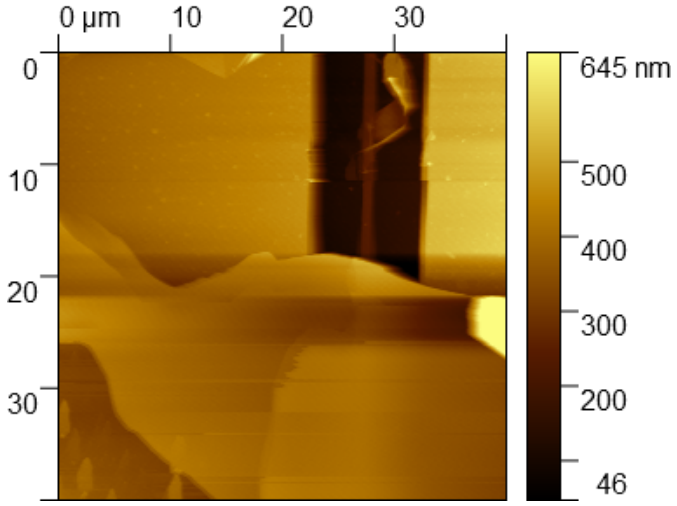

(a)

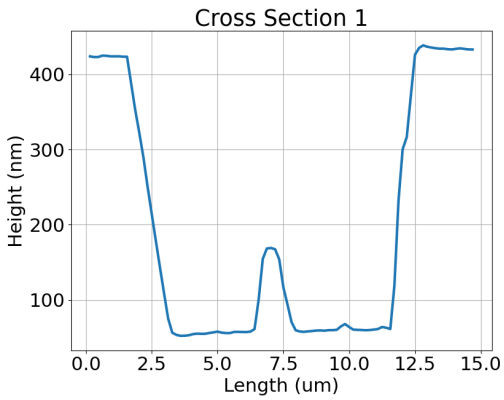

(b)

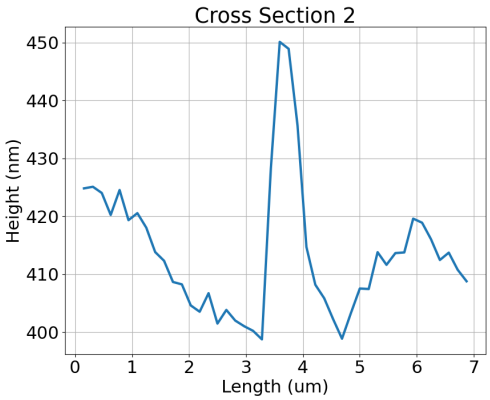

(c)

Figure 39: The topography image from an AFM with cross section graphs. The upper graph is to measure the accuracy of the AFM by going over the waveguide trench, which has known dimensions. The lower graph goes over the edge of the graphene sample which is close to the trench's left side.

The first thing to take note of when going over the interferometer measurements is that the scale is much larger than is expected from the graphene sample and waveguide the results are shown in Figure 40. The graphene sample is still in the same range as the one measured in Figure 39, which is between $20nm$ to $50nm$. Furthermore the waveguide is still $100nm$ in height which has turned into $1\mu m$ in the white light interferometer. This might be due to inaccuracies when the interferometer is creating its data set, since it does no know what materials it is measuring. However, it can be seen that the measurements in this case are ten times larger than the expected values.

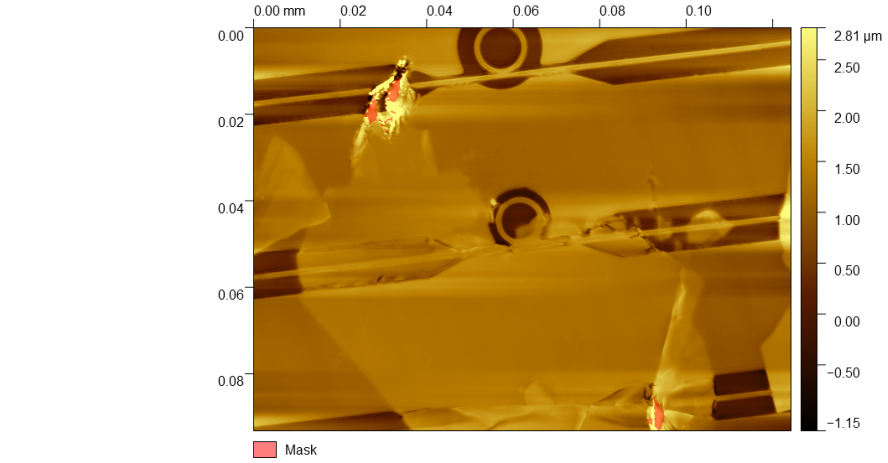

(a)

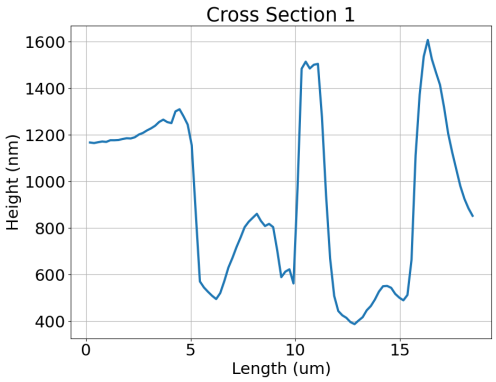

(b)

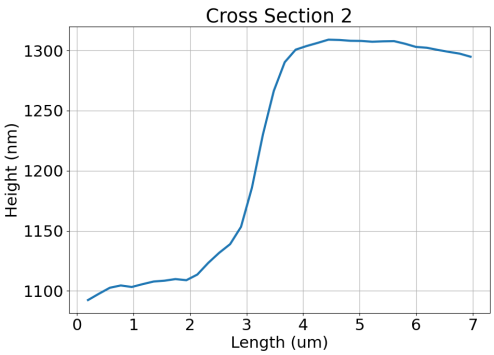

(c)

Figure 40: The topography image from a white light interferometer with cross section graphs. The upper graph is to measure the accuracy of the interferometer by going over the right waveguide trench. The lower graph goes over the edge of the graphene sample in the bottom left corner.

4 Discussion

The results show that silicon photonics can still propagate light when they are integrated with 2D membranes. However, the resonance dips, and output transmission changes after membrane transfer do lower the SNR, but, the signal is still distinguishable enough to use. Furthermore, the AFM shows that the membrane thickness is between $20nm$ and $50nm$.

4.1 Membrane Transfer

The membrane transfer was very successful when it came to transferring the membranes with only few unsuccessful transfers as seen in Figure 41 and Figure 16b. The problem with the failed transfers is that a part of the membrane is directly touching the waveguide which means that the membrane is not suspended over the guide. Thankfully, that is an uncommon problem that was observed from two situation. The first is when the membrane is not properly positioned over the device and, the second situation is when the PDMS stamp is released to early from the chip.

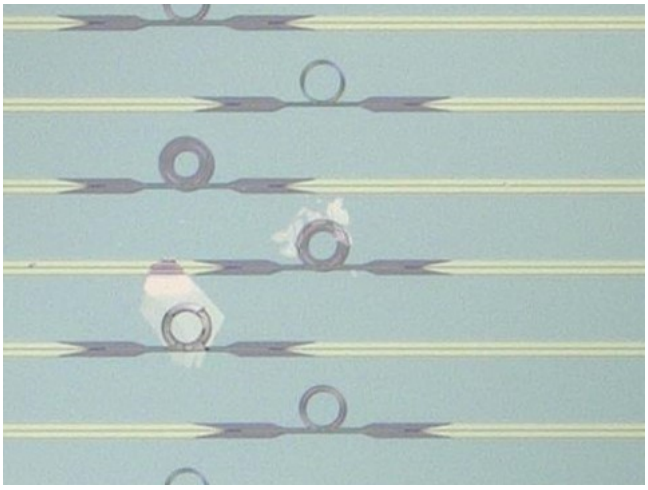

Figure 41: Die2 showing two MoS_2 transfers, where the center one is unsuccessful while the lower one is used in the study as DM71.

The more concerning part of the membrane transfers was that the waveguides in die1 were gradually breaking over the course of the study a break in a waveguide is shown in Figure 42. The new fractures were always noticed after a graphene transfer took place. Therefore, it was hypothesised that the guides were breaking during the membrane transfer process. To confirm the hypothesis, the waveguides needed to survive being stamped at least 50 times, in case the stamp it self was breaking the guides. The guides also needed to survive at least twenty cycles of a cleaning process that consists of dipping the chip in acetone, Isopropyl alcohol, and water, with ultrasonic cleaning for two minutes between chemical change and finally being dried with an air duster. The final step in the transfer process where the waveguides could break was the annealing process. The situations were independently tested by choosing a fracture free area on the chip and viewing the area between the different situations. The conclusion of these tests is that the annealing process was putting too much strain on the thin waveguides which measure between $450nm$ and $760nm$.

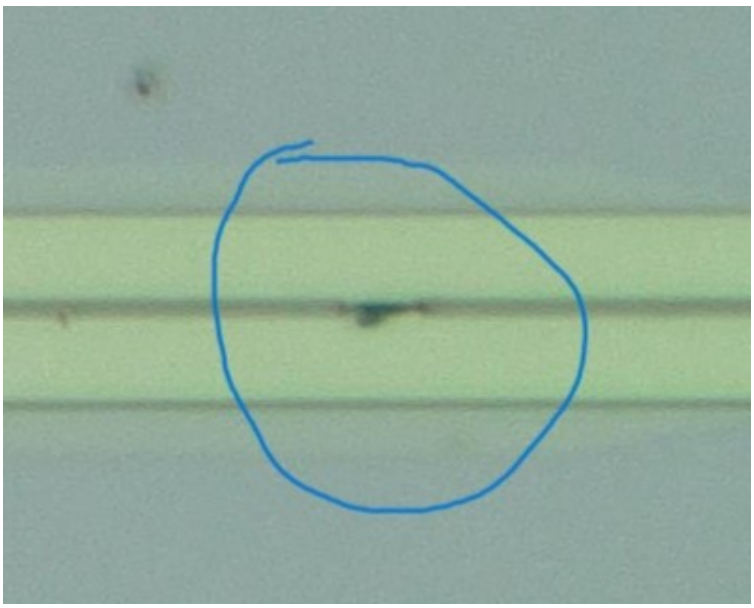

Figure 42: A break in the waveguide is seen within the circle.

4.2 The Transmission Measurements

The transmission measurements indicate that silicon photonics can detect the motion of 2D membranes. Although the measured voltage from the transmission decreased after an MoS_2 transfer the resonance dips are still distinct in Figure 35. The same cannot be said for the graphene membranes.

When looking at the results for graphene membranes. The transmission voltage collapses and the resonance dips disappear. However, there is still transmission through the straight waveguide when the graphene is covering both the straight guide and the ring resonator as seen inFigure 32.

The reason for the drop in transmission is most likely due to the graphene membrane absorbing the energy from the waveguide. Why the absorption is thought to be the culprit, is due to graphene having a constant absorption coefficient of $e^2/\epsilon_0\hbar c = 2.3\%$. Such a high coefficient can lead to total absorption when it is combined with the waveguide area that is covered by graphene as seen in Figure 16 [13]. Furthermore, S. Schuler et al showed graphene has a 90% absorption rate when the resonators are critically coupled [21]. Unfortunately, there are some devices where the graphene sunk into the waveguide trench which changes the effective and group index of the waveguide. In those cases it is light directly escaping the waveguide and the losses are then a mixture of light scattering and light absorption due to the graphene.

4.3 Fourier Transformation Analysis

When looking at the FFT results. the results are over all inconclusive. The frequency domain can very clearly show that the waveguide does not resonate in the MHz range. However, the domain cannot conclusively say that 2D membrane integrated with silicon photonics make a good sensor. Since the membrane was unfortunately not actuated before the study ended. The reason is partially due to the waveguides breaking after graphene transfer. The other part is due to not enough time given to find proper actuators or optic modulators to actuate the membrane.

When looking at the averaged frequency domain; a lot of peaks appear in the graph. These

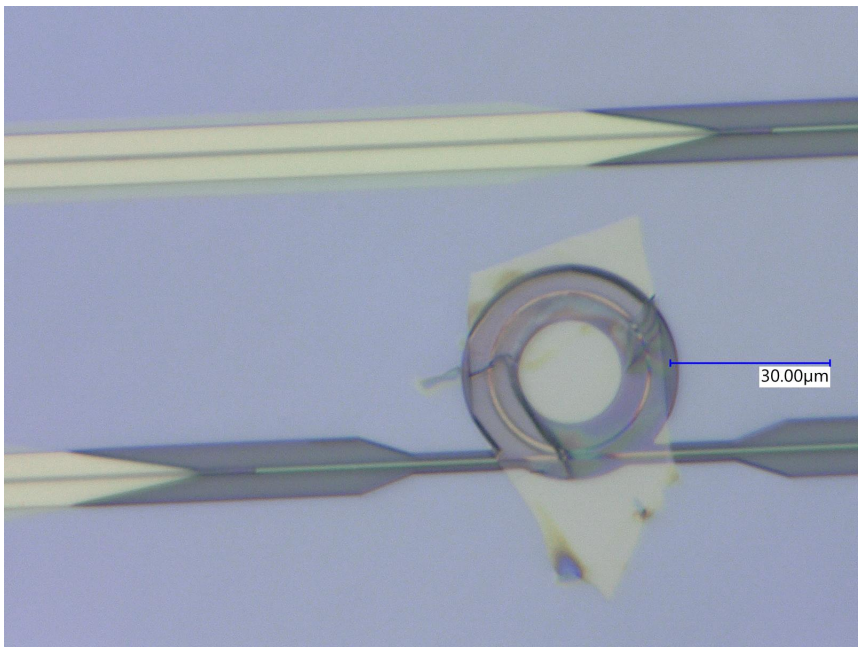

Figure 43: A waveguide where the graphene membrane has sunk into the trench. The indication comes from the shadow that is cast by the top of the suspended membrane.

peaks are perfectly staple and do not change their frequency when the measured device is changed or the device has a membrane suspended over it. Therefore, the peaks are not due to the waveguides sensitivity and are either made by the setup itself or are from the FFT algorithm that is used. Since it is harder to prove that the peaks come from the setup, a power spectral density (PSD) algorithm is used on the raw AC-signal data seen in Figure 44. Which has peaks in the exact same frequencies as the FFT algorithm does. Therefore, confirming that the peaks are most likely caused by internal resonances in the electrical connections and not by the FFT.

4.4 Recommendations

After reading the results and discussion it is clear that there are a couple of improvements to be made and the results do not give a concrete answer since the 2D membranes were never actuated. Therefore it is recommended to actuate the membrane before giving the research question a conclusive answer. The actuation should either be done with a piezoelectric actuator that is placed under the chip, or be done with an optical modulator that is placed between the laser and the chip. If a piezo is used to actuate the chip, make sure that the piezo's natural frequency is $10 \pm 4MHz$, since it is difficult to find a higher bandwidth for a piezo. Optical modulators specifically electro-optic modulators can have bandwidths exceeding $1GHz$ [4].

There are also many more devices with ring resonators on the chip that were not looked into due to their initial performance. Furthermore, since a 2D membrane affects the transmission power of the waveguides, it is possible that a suspended membrane can be placed on top of an under or over coupled device and push it closer to critical coupling. Which leads to the next recommendation since this study was more of a proof of concept, it is interesting to know which silicon photonic devices (on the chip) are the best at sensing the motion of 2D membranes.

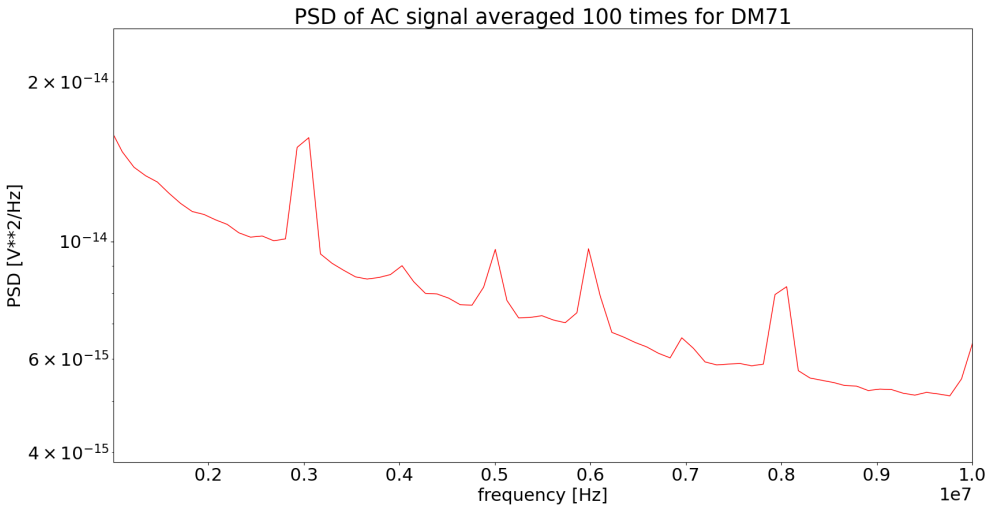

Figure 44: Power spectral density with distinguishable peaks at $3MHz$ and $6MHz$.

5 Conclusion

Silicon photonic sensors can be very small and some of the ring resonators used in the study have a radius of $5\mu m$. Which makes them ideal to make cheap and small ultrasonic sensors. Furthermore, with the open space above the waveguide, it is possible to suspend a membrane over the resonator.

Recall the research question of the thesis: "is it possible to detect 2D membrane motion with silicon photonics?" The question is quite straightforward and offers a definitive yes-or-no answer. Therefore, the goal of the research was to measure 2D membranes with a silicon waveguide. However, the original goal of the thesis was to measure the motion of graphene, unfortunately the goal changed to measuring 2D membranes in general after the results showcased that graphene membranes absorb most of the light.

Before any measurements were done on graphene membranes, a very important milestone was achieved. The milestone being a successful graphene transfer on an SOI chip. The transfer also used a newly developed method from subsubsection 2.1.2 which lets the transfer stamp cover a much smaller area of the chip compared to the old transfer method which was discussed in subsubsection 2.1.1. However, the new transfer method formed fractures in the waveguides. Therefore, it was decided to use a dry transfer method based on the new transfer method. The dry transfers were successful and there were no visible fractures in the waveguides after the transfers.

After the membrane transfers are finished, the integrated devices are ready for measurements. The first measurement after transfer is a transmission measurement as seen in Figure 32, which is compared to a transmission graph that was plotted before a membrane transfer and is seen in Figure 22. These comparisons can be enough to tell if silicon photonics can detect motion of 2D membranes. Since the comparisons are not only for the transmission power but, also how much the resonance dips change after transfer. Which leads to MoS_2 membranes that show a good example of the former statement as shown in Figure 23 and Figure 35.

Furthermore, the devices were measured with an AC-signal on their resonance dip flank wavelength. These measurements are what can truly answer the research question. Since when the

AC-signal goes under a FFT the frequency domain will show the resonating frequency of the membrane if it is moving. Unfortunately due to time constraints it was not possible to take measurements while the membrane was actuated.

The study started with the question; is it possible to detect graphene mechanics with silicon photonics? After it was discovered that the graphene absorbed the light too much. The question then asked if it is possible to detect 2D membranes with silicon photonics. And, despite not having enough time to measure the flank of the resonance dip when the membrane is actuated. The transmission results show that despite the transmission changing they are still readable, when there is a membrane on top of the waveguides. Which strongly suggests that silicon photonics can detect 2D membrane mechanics.

References

[1] Arthur W. Barnard et al. "Real-time vibrations of a carbon nanotube". In: *Nature* 566.7742 (2019), pp. 89–93. ISSN: 1476-4687.

[2] E Benavente et al. "Intercalation chemistry of molybdenum disulfide". In: *Coordination Chemistry Reviews* 224.1 (2002), pp. 87–109. ISSN: 0010-8545.

[3] Jacopo Brivio, Duncan T. L. Alexander, and Andras Kis. "Ripples and Layers in Ultrathin MoS2 Membranes". In: *Nano Letters* 11.12 (2011). PMID: 22010987, pp. 5148–5153. DOI: 10.1021/nl2022288.

[4] F Consoli et al. "Time-resolved absolute measurements by electro-optic effect of giant electromagnetic pulses due to laser-plasma interaction in nanosecond regime". In: *Sci Rep* (June 2016). DOI: 10.1038/srep27889.

[5] Aneesh Dash, S. K. Selvaraja, and A. K. Naik. "On-chip optical transduction scheme for graphene nano-electro-mechanical systems in silicon-photonic platform". In: *Opt. Lett.* 43.4 (Feb. 2018), pp. 659–662. DOI: 10.1364/OL.43.000659.

[6] Laura Garwin and Tim Lincoln, eds. *A Century of Nature: Twenty-One Discoveries that Changed Science and the World*. University of Chicago Press, 2003, pp. 107–112. ISBN: 0-226-28415-8.

[7] A. K. Geim and K. S. Novoselov. "The rise of graphene". In: *Nature Materials* 6.3 (2007), pp. 183–191. ISSN: 1476-4660.

[8] Taichi Inoue et al. "Resonance Control of a Graphene Drum Resonator in a Nonlinear Regime by a Standing Wave of Light". In: *ACS Omega* 2.9 (2017), pp. 5792–5797.

[9] Kei Kinoshita et al. "Dry release transfer of graphene and few-layer h-BN by utilizing thermoplasticity of polypropylene carbonate". In: *npj 2D Materials and Applications* 3.1 (May 2019), p. 22. ISSN: 2397-7132.

[10] Jae-Ung Lee, Duhee Yoon, and Hyeonsik Cheong. "Estimation of Young's Modulus of Graphene by Raman Spectroscopy". In: *Nano Letters* 12.9 (2012), pp. 4444–4448. DOI: 10.1021/nl301073q.

[11] S. M. Leinders et al. "A sensitive optical micro-machined ultrasound sensor (OMUS) based on a silicon photonic ring resonator on an acoustical membrane". In: *Scientific Reports* 5.1 (2015). ISSN: 2045-2322.

[12] Bei-Bei Li et al. "Cavity optomechanical sensing". In: *Nanophotonics* 10.11 (2021), pp. 2799–2832. DOI: doi:10.1515/nanoph-2021-0256. URL: https://doi.org/10.1515/nanoph-2021-0256.

[13] Huan Li et al. "Optical absorption in graphene integrated on silicon waveguides". In: *Applied Physics Letters* 101.11 (Sept. 2012), p. 111110. ISSN: 0003-6951. DOI: 10.1063/1.4752435.

[14] Xinmiao Liu et al. "Progress of optomechanical micro/nano sensors: a review". In: *International Journal of Optomechatronics* 15.1 (2021), pp. 120–159. DOI: 10.1080/15599612.2021.1986612.

[15] Qianbo Lu et al. "Investigation of a complete squeeze-film damping model for MEMS devices". In: *Microsystems & Nanoengineering* 7.1 (July 2021), p. 54.

[16] Qijie Ma et al. "Recent advances on hybrid integration of 2D materials on integrated optics platforms". In: 9.8 (2023 2020), pp. 2191–2214.

[17] Dimitrios G. Papageorgiou, Ian A. Kinloch, and Robert J. Young. "Mechanical properties of graphene and graphene-based nanocomposites". In: *Progress in Materials Science* 90 (2017), pp. 75–127. ISSN: 0079-6425. DOI: https://doi.org/10.1016/j.pmatsci.2017.07.004.

[18] Rudra Pratap, Suhas Mohite, and Ashok Pandey. "Squeeze film effects in MEMS devices". In: *Journal of the Indian Institute of Science* 87 (Jan. 2007).

[19] Graham T. Reed and Andrew P. Knights. *Silicon Photonics an Introduction*. John Wiley Sons, Ltd, 2004. ISBN: 0-470-87034-6.

[20] Sivabrata Sahu and G. C. Rout. "Band gap opening in graphene: a short theoretical study". In: *International Nano Letters* 7.2 (June 2017), pp. 81–89. ISSN: 2228-5326. DOI: 10.1007/s40089-017-0203-5.

[21] S. Schuler et al. "High-responsivity graphene photodetectors integrated on silicon microring resonators". In: *Nature Communications* 12.1 (June 2021), p. 3733. ISSN: 2041-1723. DOI: 10.1038/s41467-021-23436-x.

[22] Alexander Spott et al. "Silicon waveguides and ring resonators at 5.5m". In: *Applied Physics Letters* 97.21 (Nov. 2010), p. 213501. ISSN: 0003-6951. DOI: 10.1063/1.3514234.

[23] Peter G Steeneken et al. "Dynamics of 2D Material Membranes". In: *2D Materials* 8.4 (2021).

[24] Qing Tang and De-en Jiang. "Stabilization and Band-Gap Tuning of the 1T-MoS2 Monolayer by Covalent Functionalization". In: *Chemistry of Materials* 27.10 (2015), pp. 3743–3748.

[25] Wouter J. Westerveld and H Paul Urbach. *Silicon Photonics: Electromagnetic Theory*. IOP Publishing, 2017. ISBN: 978-0-7503-1387-2.

[26] Wouter J. Westerveld et al. "Sensitive, small, broadband and scalable optomechanical ultrasound sensor in silicon photonics". In: *Nature Photonics* 15.5 (2021), pp. 341–345. ISSN: 1749-4893.

A Annealing Setup

The annealing setup consists of a furnace, a tube, pipes, and fans.

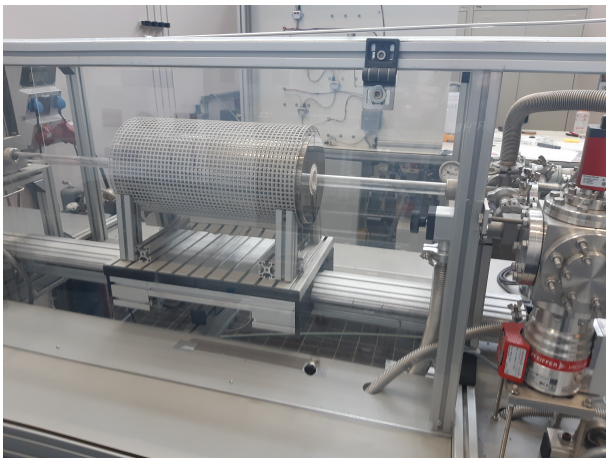

(a)

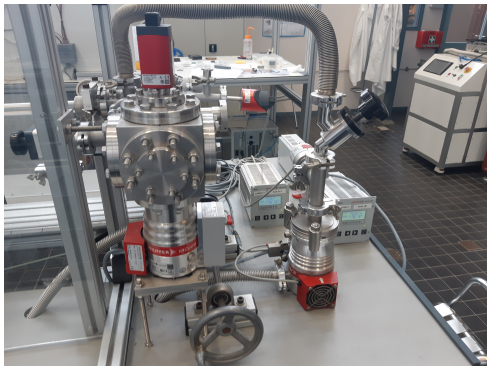

(b)

(c)

Figure 45: The annealing setup. Figure a) show the furnace drum that envelopes the vacuum tube where the chip sits during the process. Figure b) shows the vacuum connections and two turbo fans in the front. Figure c) shows the pressure readout.